

# Distinguishing among modes of convergent adaptation using population genomic data

Kristin M. Lee<sup>1,2</sup> and Graham Coop<sup>1,2</sup>

<sup>1</sup> Center for Population Biology, University of California, Davis.

<sup>2</sup> Department of Evolution and Ecology, University of California, Davis

To whom correspondence should be addressed: [krmllee@ucdavis.edu](mailto:krmllee@ucdavis.edu), [gmcoop@ucdavis.edu](mailto:gmcoop@ucdavis.edu)

## 1 Abstract

Geographically separated populations can convergently adapt to the same selection pressure. Convergent evolution at the level of a gene may arise via three distinct modes. The selected alleles can (1) have multiple independent mutational origins, (2) be shared due to shared ancestral standing variation, or (3) spread throughout subpopulations via gene flow. We present a model-based, statistical approach that utilizes genomic data to detect cases of convergent adaptation at the genetic level, identify the loci involved and distinguish among these modes. To understand the impact of convergent positive selection on neutral diversity at linked loci, we make use of the fact that hitchhiking can be modeled as an increase in the variance in neutral allele frequencies around a selected site within a population. We build on coalescent theory to show how shared hitchhiking events between subpopulations act to increase covariance in allele frequencies between subpopulations at loci near the selected site, and extend this theory under different models of migration and selection on the same standing variation. We incorporate this hitchhiking effect into a multivariate normal model of allele frequencies that also accounts for population structure. Based on this theory, we present a composite likelihood-based approach that utilizes genomic data to identify loci involved in convergence, and distinguishes among alternate modes of convergent adaptation. We illustrate our method on genome-wide polymorphism data from two distinct cases of convergent adaptation. First, we investigate the adaptation for copper toxicity tolerance in two populations of the common yellow monkeyflower, *Mimulus guttatus*. We show that selection has occurred on an allele that has been standing in these populations prior to the onset of copper mining in this region. Lastly, we apply our method to data from four populations of the killifish, *Fundulus heteroclitus*, that show very rapid convergent adaptation for tolerance to industrial pollutants. Here, we identify a single locus at which both independent mutation events and selection on very young standing variation play a role in adaptation across the species' range.

## 23 1 Introduction

Convergent adaptive evolution, where selection independently drives the evolution of the same trait, demonstrates the impressive ability of natural selection to repeatedly shape phenotypic diversity (Losos, 2011). Many studies have revealed cases of repeated adaptation resulting from changes in the same molecular mechanisms across distinct lineages (Stern, 2013; Wood et al., 2005). Here, we use the term convergence to define all cases of repeated evolution of similar traits across independent lineages, and do not distinguish between convergent and parallel evolution (Arendt and Reznick, 2008). In some cases, these convergent adaptive changes are identical at the level of the same orthologous gene or nucleotide (Martin and Orgogozo, 2013), suggesting adaptation may be more predictable and constrained than previously appreciated. Studying repeated evolution has long played a key role in evolutionary biology as a set of replicated natural experiments to help build comparative arguments for traits as adaptations, and to identify and understand the ecological and molecular basis of adaptive traits (Harvey and Pagel, 1991).

While we often think of convergent evolution among long-separated species, populations of the same (or closely-related) species often repeatedly evolve similar traits in response to similar selective pressures

37 (Arendt and Reznick, 2008). Convergent adaptation at the genetic level among closely related populations  
38 may arise via multiple, distinct modes (see Stern, 2013, for a recent review). Selected alleles present at the  
39 same loci in multiple populations can have multiple independent mutational origins (e.g. Pearce et al., 2009;  
40 Chan et al., 2010; Tishkoff et al., 2007). Alternatively, adaptation in different populations could proceed  
41 by means of selection on the standing variation present in their ancestor (e.g. Colosimo et al., 2005; Roesti  
42 et al., 2014), or a single allele spread throughout the populations via gene flow (e.g. Heliconius Genome  
43 Consortium, 2012; Song et al., 2011). Understanding the source of convergent adaptation can aid in our  
44 understanding of fundamental questions about adaptation. Distinguishing among these modes may provide  
45 evidence for how restricted the paths adaptation can take are to pleiotropic constraints and if adaptation is  
46 limited by mutational input (Orr 2005, for review). Additionally, we can improve our understanding of the  
47 role of standing variation and gene flow in adaptation (Barrett and Schluter, 2008; Hedrick, 2013; Welch and  
48 Jiggins, 2014).

49 With the advent of population genomic data, it is now possible to detect genomic regions putatively  
50 underlying recent convergent adaptations. A growing number of studies are sequencing population genomic  
51 data from closely related populations, in which some have potentially converged on an adaptive phenotype  
52 (e.g. Turner et al., 2010; Jones et al., 2012). Population genomic studies of convergent evolution often  
53 take a paired population design, sampling multiple pairs of populations that independently differ in the key  
54 phenotype or environment are sequenced. These studies are usually predicated on finding large effect loci  
55 which have rapidly increased from low frequency to identify the population genomic signal of selective sweeps  
56 shared across populations that independently share a selective pressure. Regions underlying convergent  
57 adaptations can potentially be identified by looking for genomic regions where multiple pairs of populations  
58 are strongly differentiated (e.g. using  $F_{ST}$ ) compared to the genomic background. Another broad set of  
59 approaches identify convergent loci by looking for genomic regions where the populations that share an  
60 environment cluster together phylogenetically in a way unpredicted by genome-wide patterns or geography  
61 (Pease et al., 2016; Jones et al., 2012). While these methods have proven useful in identifying loci involved  
62 in convergent adaptation, currently there are few model-based ways to identify the signal of convergence in  
63 population genomic data or to distinguish the different modes of convergent adaptation. In the case where  
64 an allele is shared due to adaptation from standing variation or migration, chunks of the haplotype on which  
65 the selected allele arose and swept on will also be shared among the populations (Slatkin and Wiehe, 1998;  
66 Bierne, 2010; Kim and Maruki, 2011; Roesti et al., 2014), providing a useful heuristic for these modes to  
67 be distinguished from convergent sweeps from independent mutations. We also note there are a variety of  
68 approaches to detect introgression (see Hedrick, 2013; Racimo et al., 2015; Rosenzweig et al., 2016, for recent  
69 reviews). However, these methods are not usually focused on detecting sweeps in both populations, but  
70 rather look for signatures of unusual amounts of shared ancestry between populations. Here, we present  
71 coalescent theory that leverages these signatures selection has on linked neutral variation in a model-based  
72 approach. We extend this to a statistical method that utilizes genomic data to identify loci involved in and  
73 distinguish between modes of genotypic convergence.

74 Positive selection impacts neutral diversity at linked loci due to hitchhiking (Maynard Smith and Haigh,  
75 1974; Kaplan et al., 1989) and can be modeled as an increase in the variance in neutral allele frequencies  
76 around their ancestral frequencies. We develop coalescent theory to show how shared hitchhiking events  
77 between subpopulations act to increase covariance in allele frequencies around their ancestral frequencies  
78 at loci near the selected site, and extend this theory under different models of migration and selection  
79 on the same standing variation. We incorporate this hitchhiking effect into a multivariate normal model  
80 of allele frequencies that also accounts for population structure, allowing for the application to data from  
81 many populations with arbitrary relationships. Based on this theory we present a composite likelihood-based  
82 approach (Kim and Stephan, 2002; Nielsen et al., 2005; Chen et al., 2010; Racimo, 2016) that utilizes genomic  
83 single-nucleotide polymorphism (SNP) data to identify loci involved in convergence, and distinguishes among  
84 alternate modes of convergent adaptation. As these models are also specified by relevant parameters, it is  
85 possible to obtain estimates for parameters of interest such as the strength of selection, the minimum age  
86 and frequency of a standing variant, and the source population of the beneficial allele in cases of migration.

87 This method should be of wide use with the increase in population genomic samples from across the  
88 geographic range of a species. Here, we illustrate the utility of our inference method by applying it to  
89 genome-wide polymorphism data from two distinct cases of convergent adaptation. First, we investigate the  
90 basis of the convergent adaptation observed across populations of the annual wildflower *Mimulus guttatus* to

91 copper contaminated soils from two populations sampled near Copperopolis, California (Wright et al., 2015).  
92 We find selection has been acting on standing variation shared between these populations for a tolerance  
93 allele present prior to the onset of copper mining in this region. To further exemplify the flexibility of our  
94 method, we study a more complex population scenario: the rapid adaptation of four populations of killifish  
95 (*Fundulus heteroclitus*) to high levels of pollution, sampled across the Eastern seaboard of the United States  
96 (Reid et al., 2016). We find that even at the level of a single gene, both selection on very young shared  
97 standing variation and convergent mutation have played a role in adaptation in this species.

## 98 2 Models

99 In the following section, we present models for the three modes of genotypic convergent adaptation: (1)  
100 multiple independent mutations at the same locus, (2) selection on shared ancestral standing variation, and  
101 (3) migration between populations spreading a beneficial allele. Throughout this section, we compare our  
102 derived expectations to coalescent simulations using mssel, a modified version of ms (Hudson, 2002) that  
103 allows for the incorporation of selection at a single site. This simulation program takes as input the frequency  
104 trajectory of the selected allele for each population. We specify stochastic trajectories of the selected allele  
105 in populations following our three modes of convergence (see Appendix A.2 for simulation details). We  
106 focus on a set of four populations as shown in Figure 1 where populations 2 and 3 are adapted to a shared  
107 novel selection pressure and populations 1 and 4 are in the ancestral environment. The average coancestry  
108 coefficient values across simulations, estimated as described in Appendix A.1, are plotted for 100 bins of  
109 recombination distance away from the selected site, which occurs at distance 0. The results for all three  
110 models are shown in dashed lines in Figure 3.

### 111 2.1 Null Model

112 We aim to model the variances and covariances of the neutral allele frequencies within and between popula-  
113 tions due to convergent sweeps. First, we must specify a null model that accounts for population structure.  
114 Populations will have some level of shared deviations away from an ancestral allele frequency,  $\epsilon$ , due to shared  
115 genetic drift. Let  $x_i$  represent the present day allele frequency in population  $i$  (Figure 1). We denote the  
116 deviation of this frequency from the ancestral frequency by  $\Delta x_i = x_i - \epsilon$ . Genetic drift, in expectation across  
117 loci, does not change the population allele frequencies (i.e.  $\mathbb{E}[\Delta x_i] = 0$ ) as an allele increases or decreases  
118 in frequency with equal probability. Drift however does act to increase the variance in this deviation across  
119 loci, with this variance increasing as more time is allowed for drift. The variance in the change of neutral  
120 allele frequencies in population  $i$  is

$$\text{Var}[\Delta x_i] = \mathbb{E}[\Delta x_i^2] = \epsilon(1 - \epsilon)f_{ii} \quad (1)$$

121 where  $f_{ii}$  can be thought of as the genetic drift branch length leading from the ancestral population to  
122 population  $i$  (Nicholson et al., 2002), specifying how much allele frequencies in population  $i$  deviate from  
123 their ancestral values (Figure 1). By rearranging Equation 1,  $f_{ii}$  can be interpreted as the population-specific  
124  $F_{ST}$  for population  $i$  relative to the total population, here represented by the ancestral population (Wright,  
125 1943, 1951; Weir and Hill, 2002; Nicholson et al., 2002).

126 Populations covary in their deviations from  $\epsilon$  as some populations are more closely related due to shared  
127 genetic drift resulting from shared population history or gene flow. The covariance in this deviation between  
128 populations  $i$  and  $j$  is

$$\text{Cov}[\Delta x_i, \Delta x_j] = \mathbb{E}[\Delta x_i \Delta x_j] = \epsilon(1 - \epsilon)f_{ij} \quad (2)$$

129 where  $f_{ij}$  is interpreted as the coancestry coefficient between populations  $i$  and  $j$ , and can be thought of as  
130 the shared branch length connecting  $i$  and  $j$  to the ancestral population (Figure 1).

131 Other natural interpretations of  $f_{ii}$  and  $f_{ij}$  follow from these definitions. Specifically, these values are  
132 probabilities of a pair of lineages being identical by descent relative to the ancestral population, i.e. the  
133 probability two sampled lineages coalesce before reaching the ancestral population (see Thompson, 2013, for  
134 a recent review). We briefly review this coalescent interpretation in Appendix A.1. For  $f_{ii}$  these two lineages  
135 are sampled both from population  $i$ . For  $f_{ij}$ , one lineage is sampled from population  $i$  and the other from  
136 population  $j$ . We note that in practice we do not get to observe the ancestral frequency, nor may the history

137 of our populations be well represented by a tree-like structure. However, for the sake of clarity, we proceed  
 138 with these assumptions and deal with these complications in the implementation of the method.

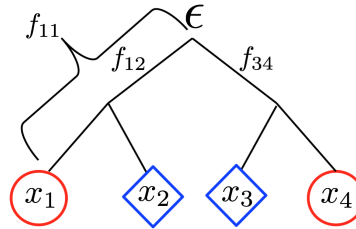


Figure 1: Present day population allele frequencies at a given neutral locus ( $x_1$ – $x_4$  for populations 1–4, respectively) are derived from ancestral allele frequency  $\epsilon$ . Each population has a coancestry coefficient proportional to the amount of drift experienced since the split from the ancestral population.  $f_{11}$  is shown for population 1. Here, populations 1 and 2, and 3 and 4 share drift relative to the ancestral population and have nonzero coancestry coefficients  $f_{12}$  and  $f_{34}$ , respectively. Blue diamonds represent the novel selective environment and red circles the ancestral environment.

We define a matrix,  $\mathbf{F}$ , for  $K$  populations as a  $K \times K$  matrix of coancestry coefficients. For example, for the four populations shown in Figure 1, this matrix takes the following form:

$$\mathbf{F} = \begin{bmatrix} f_{11} & f_{12} & 0 & 0 \\ f_{12} & f_{22} & 0 & 0 \\ 0 & 0 & f_{33} & f_{34} \\ 0 & 0 & f_{34} & f_{44} \end{bmatrix}$$

139 Populations  $i$  and  $j$  that split after the ancestral population and share no additional drift (e.g. populations  
 140 1 and 3) have  $f_{ij} = 0$  by definition.

## 141 2.2 Incorporating selection

142 Positive selection impacts neutral diversity at linked loci due to hitchhiking. As the beneficial allele increases  
 143 rapidly in frequency, so does the haplotype on which it arose. Neutral alleles further from the selected site  
 144 may recombine off the selected background during the sweep, whose duration depends on the strength of  
 145 selection. The effect of hitchhiking on the changes of linked neutral allele frequencies is similar to that of  
 146 genetic drift. Hitchhiking does not alter the expected frequency change of linked neutral alleles across loci  
 147 (i.e.  $\mathbb{E}[\Delta x_i] = 0$ ) because the selected mutation arises on a random haplotypic background. Moreover,  
 148 Hitchhiking increases the variance in the deviation in neutral allele frequencies away from their ancestral  
 149 values ( $\text{Var}[\Delta x_i]$ ) at linked sites (Gillespie, 2000). Shared hitchhiking events between subpopulations will  
 150 act to increase covariance in allele frequency deviations between subpopulations ( $\text{Cov}[\Delta x_i, \Delta x_j]$ ) at loci  
 151 near the selected site. This effect of hitchhiking on linked diversity, within and among populations gives us  
 152 a way to distinguish among alternate modes of convergent adaptation.

153 We define new matrices of coancestry coefficients that incorporate selection in addition to drift as  $\mathbf{F}^{(S)}$ .  
 154 In the following section, we use a coalescent approach to derive coancestry coefficients within and between  
 155 populations,  $f_{ii}^{(S)}$  and  $f_{ij}^{(S)}$ , for the three modes of genotypic convergent adaptation (Figure 2). In Appendix  
 156 A.5 we derive some of the same results forwards in time to help guide the reader’s intuition. Note that all  
 157 our models of selection are phrased in terms of distortions to the neutral matrix  $\mathbf{F}$ ; therefore, the precise  
 158 source of the neutral population structure (e.g. whether its due to shared population history or migration)  
 159 is relatively unimportant to our approach. A deeper knowledge of the basis of this structure does add to the  
 160 interpretation of the results, as we explain in the discussion.

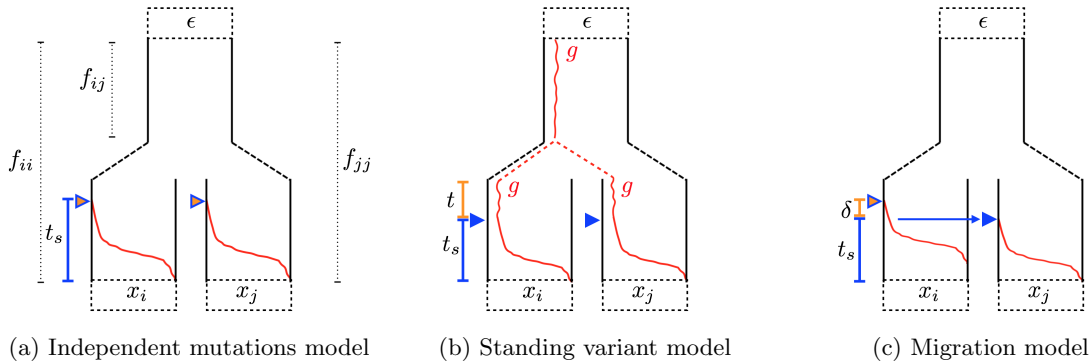


Figure 2: Trajectories of the beneficial allele (red) for the three modes of convergent adaptation. Populations  $i$  and  $j$  are under selection with present-day allele frequencies  $x_i$  and  $x_j$  at a neutral locus, derived from an ancestral population with allele frequency  $\epsilon$ . The populations share some amount of drift proportional to  $f_{ij}$  before reaching the ancestral population. (2a) Beneficial mutations, indicated by the orange triangles, occur independently in the selected populations after they have become isolated. Selection begins, indicated by the blue triangles, once the beneficial allele is present in the population. The beneficial allele sweep to fixation in  $t_s$  generations. (2b) The beneficial allele is standing at frequency  $g$  in the ancestral population. After the selected populations split, it is still standing at frequency  $g$  for  $t$  generations prior to the onset of selection. (2c) The beneficial allele arises in population  $i$  and begins sweeping in population  $i$ . Meanwhile, there is a continuous low level of migration from population  $i$  into population  $j$ . The beneficial allele establishes in  $j$  after  $\delta$  generations, where it is swept to fixation in  $t_s$  generations.

## 161 2.2.1 Independent mutation model

162 We first consider the case when a beneficial allele arises independently via *de novo* mutations at the same  
 163 locus, or tightly linked loci, in both of the selected populations. We expect hitchhiking to increase the  
 164 variance in neutral allele frequency deviations around the selected site in both populations. However, as the  
 165 sweeps are independent and there is no gene flow between populations during or after the sweep, we expect  
 166 no covariance in the neutral allele frequency deviations between these populations, beyond that expected  
 167 under neutrality due to shared population history prior to the introduction of the beneficial allele.

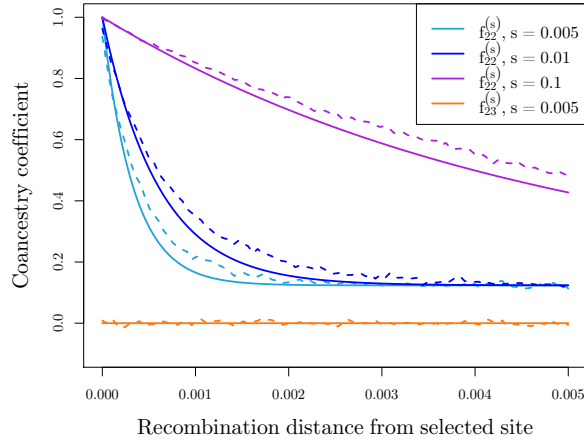
168 Moving backward in time, sampled neutral lineages linked to the selected site will be forced to coalesce  
 169 if both lineages do not recombine off the sweep. We define the probability that a single neutral allele fails to  
 170 recombine off the background of the beneficial allele during the sweep phase as  $y$ , which we can approximate  
 171 as

$$y \approx e^{-rt_s/2} \quad (3)$$

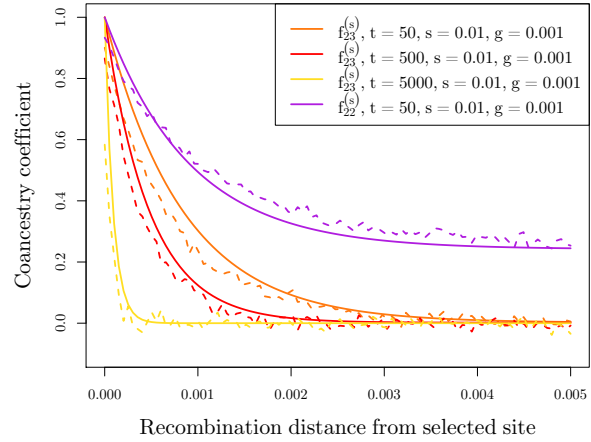
172 where  $r$  is the recombination rate between the neutral locus and selected site, and  $t_s$  is the amount of time  
 173 the sweep phase takes (Figure 2a). When the beneficial allele arises from a new mutation and selection is  
 174 additive,  $t_s \approx 2\log(4N_e s)/s$ , where  $s$  is the selection coefficient for the heterozygote, such that heterozygotes  
 175 experience a selective advantage of  $s$  and homozygotes  $2s$  (Gillespie, 2000; Barton, 1998). The factor of  $4N_e s$   
 176 is due to the fact that our new mutation, if it is to establish in the population, rapidly reaches frequency  
 177  $1/(4N_e s)$  in the population and then increases deterministically from that frequency (Maynard Smith, 1971;  
 178 Barton, 1998; Kim and Nielsen, 2004).

179 The coancestry coefficient in population  $i$  that experiences a sweep,  $f_{ii}^{(S)}$ , is defined as the probability  
 180 that two lineages sampled from population  $i$  coalesce either due to the sweep phase or neutrally before  
 181 reaching the ancestral population. With probability  $y^2$ , both lineages fail to recombine off the beneficial  
 182 background during the sweep, and they will be forced to coalesce. If one or both lineages recombines off the  
 183 sweep (with probability  $1 - y^2$ ), they can coalesce before reaching the ancestral population with probability  
 184  $f_{ii}$ . Combining these we find

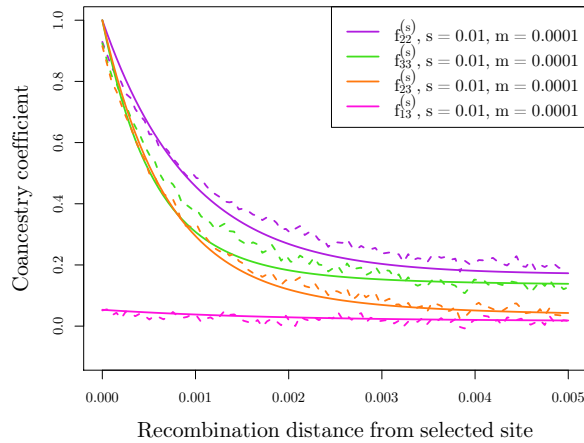
$$f_{ii}^{(S)} = y^2 + (1 - y^2)f_{ii} \quad (4)$$



(a) Independent mutations model



(b) Standing variant model



(c) Migration model

Figure 3: We calculated the average coancestry coefficient values across 1000 runs of simulations for each of 100 bins of distance away from the selected site to compare our simulation results (dashed lines) to our theoretical expectations (solid lines). (3a) Average coancestry coefficients under the independent mutations model ( $N_e = 100,000$ ) within a selected population (population 2) with varying  $s$ . Also shown is the coancestry coefficient between selected populations which in this case is 0, the neutral expectation. (3b.) Coancestry coefficients under the standing variation model between selected populations with varying amount of time beneficial allele has been independently standing in populations ( $t$ ). The coancestry coefficient within a single population is also shown for  $t = 50$ . For all,  $N_e = 10,000$ ,  $g = 0.001$ ,  $s = 0.01$ . (3c) Coancestry coefficients under the migration model, within both selected populations (source population 2 and recipient population 3) as well as between source and recipient (2,3) and between recipient and a non-selected population (1,3). Here we are showing one set of parameters ( $s = 0.01$ ,  $m = 0.001$ ,  $N_e = 10,000$ ) as estimates do not vary dramatically with changing  $m$  (see Figure S2).

185 For the coancestry coefficient between two selected populations  $i$  and  $j$ , we can calculate the probability  
186 two lineages, one sampled from population  $i$  and the other from population  $j$ , coalesce. When the sweeps  
187 are independent, the lineages can only coalesce with probability  $f_{ij}$  before reaching the ancestral population,  
188 as they have no probability of coalescing during the sweep phases which have independent origins. Thus,

$$f_{ij}^{(S)} = f_{ij} \quad (5)$$

189 **Comparison to simulated data** In Figure 3a we show the case of convergence due to independent  
190 origins of the beneficial allele. As we predicted there is no additional coancestry between the selected  
191 populations. Additionally, we show how the coancestry within a selected population decays with distance  
192 from the selected site for a range of values for the strength of selection. These coancestry values decay to the  
193 neutral expectation at other regions of the genome. With larger  $s$ , this decay is slower as the sweep occurs  
194 more rapidly and there are fewer chances for recombination to occur during this time.

### 195 2.2.2 Standing variant model

196 We turn now to the case of a sweep shared between populations  $i$  and  $j$  due to selection acting on shared  
197 ancestral variation (Figure 2b). Our model is appropriate for cases where the standing variation from which  
198 the sweep arises was previously neutral or was maintained in the population at some low frequency by  
199 balancing selection. Let the beneficial allele be standing at frequency  $g$  in the ancestral population. We  
200 assume that the beneficial allele frequency does not deviate much from that of the ancestral population such  
201 that it is still  $g$  in the daughter populations prior to selection. Selection favoring the beneficial alleles begins  
202  $t$  generations after the populations split and the beneficial allele reaches fixation in both populations after  
203  $t_s$  generations (see Figure 2b).

204 We first consider the coalescent process of two lineages within a single selected population. Again,  $y$  is  
205 the probability that a neutral lineage fails to recombine off the background of the beneficial allele during  
206 the sweep phase. Given that the beneficial allele is increasing from frequency  $g$ ,  $y$  takes the same form as  
207 Equation 3, where now  $t_s \approx 2 \log(1/g)/s$ . If both lineages fail to recombine off the beneficial background  
208 during the sweep, there is a probability of coalescing during the standing phase that is higher than the  
209 probability of two neutral lineages randomly sampled from the population coalescing. Following from our  
210 assumptions during the standing phase, the rate at which two lineages coalesce within a population is  
211  $1/(2N_e g)$  per generation. Alternatively, a lineage can recombine off in the standing phase onto the other  
212 background with probability  $r(1-g) \approx r$  per generation. As these are two competing exponential processes,  
213 the probability two lineages coalesce before either recombines off the beneficial background can be simplified  
214 to

$$\text{P(coalesce in standing phase)} = \frac{1}{1 + 4N_e r g} \quad (6)$$

215 as described by Berg and Coop (2015). If either neutral lineage recombines off the beneficial background  
216 before they coalesce, the probability of coalescing with the other lineage before reaching the ancestral popu-  
217 lation can be treated as the coancestry coefficient associated with that particular portion of the population  
218 tree.

219 Taking these approximations into account, we derive a coancestry coefficient for a neutral allele in popu-  
220 lation  $i$  that experiences selection from standing variation as

$$f_{ii}^{(S)} = y^2 \left( \frac{1}{1 + 4N_e r g} + \frac{4N_e r g}{1 + 4N_e r g} f_{ii} \right) + (1 - y^2) f_{ii} \quad (7)$$

221 The first term corresponds to both lineages failing to recombine off the beneficial background during the  
222 sweep phase, which puts them both on the same background as the beneficial allele in the standing phase.  
223 Now, the two lineages can either coalesce in the standing phase or recombine off of the background of the  
224 beneficial allele where they can coalesce neutrally before they reach the ancestral population. Alternatively,  
225 one or both lineages can recombine off during the sweep phase and again they can coalesce neutrally.

226 Populations that share a sweep due to shared standing ancestral variation will have increased covariance  
227 in the deviations of neutral allele frequencies around their ancestral means around the selected site since  
228 they will have a shared segment of the swept haplotype. From a coalescent perspective, this occurs because

229 two lineages sampled from each population have a higher probability of coalescing if they stay on the  
230 beneficial background during the sweep and standing phases than two lineages sampled randomly between  
231 the populations.

232 The probability that a single lineage does not recombine off onto the non-beneficial background during  
233 the standing phase for  $t$  generations can be approximated as

$$r_t = (1 - r(1 - g))^t \approx e^{-rt} \quad (8)$$

234 The coancestry coefficient between populations  $i$  and  $j$  is now

$$f_{ij}^{(S)} = y^2 \left( r_t^2 \left( \frac{1}{1 + 4N_e r g} + \frac{4N_e r g}{1 + 4N_e r g} f_{ij} \right) + (1 - r_t^2) f_{ij} \right) + (1 - y^2) f_{ij}. \quad (9)$$

235 This derivation follows from that of  $f_{ii}^{(S)}$  in Equation 7, but now incorporates the additional probability  $r_t^2$   
236 of both lineages failing to recombine off the beneficial background during their independent standing phases  
237 for time  $t$ .

238 These results hold when we have a simple tree as in Figure 1. However, for more complex models, it  
239 is necessary to incorporate a model that has the standing allele spreading by migration from some source  
240 population to recipient populations  $t$  generations in the past. See A.3 for details. This model differs from the  
241 migration model presented in the next section in which we assume a continuous rate of migration throughout  
242 the duration of the sweep and that the variants sweep as soon as they are established in the population. In  
243 this standing case with a source of the standing variant, moving backwards in time we assume that the allele  
244 is standing for  $t$  generations in a population after the sweep and before the beneficial lineage migrates back  
245 instantly into a specified source population (see Figure 11). This is done to formally specify the changes  
246 in coancestries between selected and non-selected populations as well as between selected populations when  
247 there are multiple pairs to generate self-consistent covariance matrices. Biologically, it naturally captures  
248 the case where the allele is shared between the populations due to migration but is standing for sometime  
249 before it sweeps.

250 **Comparison to simulated data** In Figure 3b we show comparisons of simulations to show the fit of  
251 our predictions to simulations with adaptation from standing variation. As the duration of the independent  
252 standing phases,  $t$ , increases, the coancestry at linked neutral alleles between selected populations decreases.  
253 Forward in time, this has the interpretation that the longer the beneficial allele is standing in the populations,  
254 the shorter the shared haplotype between the populations will be due to independent recombination events  
255 before selection begins. In the case that the beneficial allele has been standing for a very long time ( $t \rightarrow \infty$ )  
256 before selection occurs, this additional covariance will reduce to zero as in the independent sweeps case  
257 (Equation 5). Conversely, if the standing variant is very young ( $t \rightarrow 0$ ), the decay in covariance between  
258 populations takes the form of the variance within populations (Equation 7) which, as we will see in the next  
259 section, looks similar to the pattern generated under the migration model.

### 260 2.2.3 Migration model

261 We now consider the case where the selected allele is spread across sub-populations by migration. This  
262 scenario has been studied by a number of authors (Slatkin and Wiehe, 1998; Santiago and Caballero, 2005;  
263 Kim and Maruki, 2011), and our approach here follows similar lines to that of Kim and Maruki (2011). Let  
264 there be a single origin of the beneficial allele, which occurs in population  $i$ . We assume a low, continuous level  
265 of migration during the sweep, with a proportion  $m$  of individuals in population  $j$  coming from population  
266  $i$  each generation. We say the sweep began in population  $j$  at time  $t_s$  generations in the past and at time  
267  $t_s + \delta$  for population  $i$  (Figure 2c). Kim and Maruki (2011) found that the mean delay time,  $\delta$ , between the  
268 two sweeps can be approximated by

$$\delta \approx \frac{1}{s} \log \left( 1 + \frac{s}{m} \right). \quad (10)$$

269 The coancestry coefficient of the source population,  $f_{ii}^{(S)}$ , follows that of a population experiencing an  
270 independent sweep from new mutation (Equation 4). To derive the coancestry coefficient of the recipient



271 population,  $f_{jj}^{(S)}$ , we first need to consider the fate of two lineages sampled in population  $j$  at the selected  
 272 site. Two events can occur if we trace the lineages of two beneficial alleles back in time: either the two  
 273 lineages coalesce in population  $j$  and a single lineage migrates back into population  $i$  or the two lineages  
 274 independently migrate back into the source population and coalesce there. We define the probability of these  
 275 two events as  $Q$  and  $1 - Q$ , respectively. We use the approximation

$$Q \approx \frac{1}{1 + 4Nm} \quad (11)$$

276 (see Pennings and Hermisson, 2006). Assuming  $m$  is small, such that a beneficial allele sampled at present  
 277 day in population  $j$  migrates back into population  $i$  approximately  $t_s$  generations in the past, the probability  
 278 of a linked neutral allele recombining off during the sweep phase in population  $j$  can be approximated by  $y$ .  
 279 If the lineage migrates back into population  $i$  before it recombines off the beneficial background, there is an  
 280 additional time  $\delta$  in population  $i$  for recombination to happen. So, there is an additional probability,  $e^{-r\delta}$ ,  
 281 of recombination of our linked neutral allele off the beneficial background.

282 Thus, the coancestry coefficient for the recipient population is now

$$f_{jj}^{(S)} = Q\left(y^2 + (1 - y^2)f_{jj}\right) + (1 - Q)\left(y^2e^{-2r\delta} + y^2(1 - e^{-2r\delta})f_{ii} + 2(1 - y)yf_{ij} + (1 - y)^2f_{jj}\right) \quad (12)$$

283 The terms in this approximation correspond to the following coalescent scenarios: First, if two lineages  
 284 sampled in population  $j$  coalesce before migrating (with probability  $Q$ ), then linked neutral alleles can  
 285 coalesce either during the sweep if neither lineage recombines off the beneficial background or neutrally if  
 286 either lineage recombines off. Alternatively, if the two lineages fail to coalesce before one or both migrates  
 287 (w.p.  $1 - Q$ ), there are four ways linked neutral alleles can coalesce:

- 288 1. Both lineages fail to recombine off the beneficial background during the sweep and are forced to  
 289 coalesce during the sweep in population  $i$ . The factor  $e^{-2r\delta}$  represents the additional opportunity for  
 290 recombination when both lineages have migrated back into population  $i$ .
- 291 2. Both lineages stay on the beneficial background in population  $j$  (w.p.  $y^2$ ) but one or both lineages  
 292 recombines off in population  $i$  (w.p.  $1 - e^{-2r\delta}$ ) and they coalesce neutrally in the source population  
 293 with probability  $f_{ii}$  before reaching the ancestral population.
- 294 3. Either lineage recombines off the beneficial background while it is still in population  $j$  and the two  
 295 lineages coalesce neutrally in the shared drift phase of populations  $i$  and  $j$ , with probability  $f_{ij}$  before  
 296 reaching the ancestral population.
- 297 4. Both lineages recombine off during the sweep phase while they are still in population  $j$  and they coalesce  
 298 neutrally with probability  $f_{jj}$ .

299 When a beneficial allele is shared between populations  $i$  and  $j$  via migration, there will be additional  
 300 covariance in the deviations of linked neutral allele frequencies from their ancestral means. In this case,  
 301 there are three ways a lineage sampled from population  $i$  and a lineage sampled from population  $j$  can  
 302 coalesce. They are forced to coalesce during the sweep if both lineages fail to recombine off the background  
 303 of the sweep, which occurs with probability  $y^2e^{-r\delta}$ . Alternatively, the lineage sampled in population  $j$  can  
 304 recombine off the beneficial background before it migrates back to source population  $i$ , in which case the  
 305 lineages can coalesce neutrally before reaching the ancestral population in their shared drift phase, with  
 306 probability  $f_{ij}$ . Lastly, if the lineage sampled in population  $j$  migrates back into population  $i$  then the  
 307 two sampled neutral lineages can coalesce neutrally in population  $i$  with probability  $f_{ii}$  if the lineages don't  
 308 coalesce due to the sweep (i.e. either recombines off in time  $t_s$  or  $\delta$ ). Thus, in the case of continuous  
 309 migration the coancestry coefficient between the source and recipient population is

$$f_{ij}^{(S)} = y^2e^{-r\delta} + (1 - y)f_{ij} + y(1 - ye^{-r\delta})f_{ii} \quad (13)$$

310 To fully specify the coancestry matrix with selection, we need to take into account the effect migration  
 311 has on non-selected populations. Specifically, the coancestry coefficients between recipient and non-selected  
 312 populations are impacted since there is some probability linked neutral lineages will migrate from the recipient

313 population into the source population backwards in time. Let population  $k$  be a non-selected population.  
 314 Now, the coancestry coefficient between populations  $j$  and  $k$  can be expressed as

$$f_{jk}^{(S)} = (1 - y)f_{jk} + yf_{ik} \quad (14)$$

315 This is informative about the direction of migration. First, there is no impact of selection on the re-  
 316 lationship between the source and non-selected populations. Additionally, the sweep shared via migration  
 317 will induce additional coancestry between  $j$  and  $k$  if  $k$  is more closely related to our source population (e.g.  
 318 population 1 in Figure 1 if population 2 is the source). The opposite is true if  $k$  is more closely related to  
 319 our recipient population (e.g. population 4). Now, there is a deficit in the background level of coancestry  
 320 between populations  $j$  and  $k$  near the selected site.

321 **Comparison to simulated data** In Figure 3c we show our results above compared to simulations with  
 322 migration, for a single set of parameters ( $s = 0.01$ ,  $m = 0.001$ ). Here, we have migration occurring from  
 323 population 2 into population 3. We show the four relevant coancestries as a function of distance from the  
 324 selected site: the covariance within source ( $f_{22}^{(S)}$ ), within recipient ( $f_{33}^{(S)}$ ), between source and recipient ( $f_{23}^{(S)}$ ),  
 325 within recipient and a non-selected population ( $f_{13}^{(S)}$ ). We see the coancestry within the recipient population  
 326 decays more rapidly than coancestry within the source population. This fits our expectations as there  
 327 is some probability a lineage will, backwards in time, migrate back to the source population, decreasing  
 328 the probability of coalescing before reaching the ancestral population when  $m$  is small. As  $m$  increases,  
 329 this relationship changes (Figure S2). We also see increased coancestry near the selected site between the  
 330 selected populations. The pattern of decay varies from that observed in our standing variation model,  
 331 except for when  $t$  is small. Additionally, we see increased coancestry between the recipient population and  
 332 a non-selected population that decays with recombinational distance to their neutral expectation. Note,  
 333 the reverse, coancestry recovering to the neutral expectation with recombinational distance is observed for  
 334 populations that initially are more related to the recipient population (i.e. population 4), is also seen (Figure  
 335 S3a). The coancestries between the source population and non-selected populations are unaffected (Figure  
 336 S3b). Together, these observations using information from non-selected populations help distinguish possible  
 337 source populations.

### 338 3 Inference

339 We have described how selection at linked loci affects the matrix of coancestry coefficients, allowing us to  
 340 parameterize the variance and covariance in neutral allele frequency deviations within and between popu-  
 341 lations. To estimate the likelihood of our data under convergent adaptation models, we need a probability  
 342 model for how allele frequencies depend on these variances and covariances. Neutral allele frequencies across  
 343  $K$  populations can approximately be modeled jointly as a multivariate normal distribution around the an-  
 344 cestral allele frequency,  $\epsilon$ , with covariance proportional to the coancestry coefficients (Nicholson et al., 2002;  
 345 Weir and Hill, 2002; Coop et al., 2010; Samanta et al., 2009). Specifically,

$$\vec{x} \sim \mathcal{N}(\epsilon \vec{1}, \epsilon(1 - \epsilon)\mathbf{F}) \quad (15)$$

346 where  $\vec{x}$  is a vector of population frequencies and  $\mathbf{F}$  is the  $K$  by  $K$  matrix of coancestry coefficients without  
 347 selection.

348 Above we demonstrated that we can generate coancestry matrices  $\mathbf{F}^{(S)}$  to explain the coancestry between  
 349 multiple populations due to neutral processes and various modes of convergent adaptation.  $\mathbf{F}^{(S)}$  is a function  
 350 of the neutral coancestry, ( $\mathbf{F}$ ) the model of convergence ( $M$ ) and its parameters ( $\Theta_M$ ), and the recombination  
 351 distance a neutral site is away from a selected site ( $r_l$ ). Thus, modeling neutral allele frequencies as multi-  
 352 variate normal with covariance proportional to this new coancestry matrix, we can calculate the likelihood  
 353 of observed data a given distance away from the selected site under a specific model of convergence as

$$P(\vec{x}_l | r_l, \mathbf{F}, M, \Theta_M) \approx \mathcal{N}(\vec{x}_l | \epsilon_l \vec{1}, \epsilon_l(1 - \epsilon_l)\mathbf{F}^{(S)}(r_l, \mathbf{F}, M, \Theta_M)) \quad (16)$$

354 In practice, we do not know the true ancestral mean at a given locus,  $\epsilon_\ell$ , so we use the mean of the  
 355 present day population allele frequencies and calculate likelihoods of mean-centered allele frequencies and  
 356 coancestry matrices (we account for this mean centering in appendix A.2.6). We also do not know the true  
 357 neutral coancestry matrix,  $\mathbf{F}$ , but estimate it from deviations of allele frequencies from sample means across  
 358 the entire genome. We also incorporate the effects of sampling into this variance-covariance matrix. See  
 359 appendix A.1 for details.

### 360 3.1 Composite likelihood framework

361 We calculate the likelihood of all data ( $D_\ell$ ) in a large window around the selected site ( $\ell$ ) under a given  
 362 model of convergent adaptation ( $M$ ), with its associated parameters ( $\Theta_M$ ), as the product of the marginal  
 363 likelihoods for sites all distances away from the selected site. This composite likelihood is used as an  
 364 approximation to the total likelihood of all sites, but is not a proper likelihood as neighboring sites are  
 365 correlated due to shared histories. Moving  $L_{\text{left}}$  sites to the left of the proposed selected site and  $L_{\text{right}}$  sites  
 366 to the right,

$$\mathcal{L}_C(M, \Theta_M; D_\ell) = \prod_{i=1}^{L_{\text{left}}} P(\vec{x}_i | M, \mathbf{F}_M^{(S)}(r_i, \mathbf{F}, M, \Theta_M)) \prod_{j=1}^{L_{\text{right}}} P(\vec{x}_j | \mathbf{F}_M^{(S)}(r_j, \mathbf{F}, M, \Theta_M)) \quad (17)$$

367 where  $r_i$  is the genetic distance from site  $i$  to  $\ell$ , and similarly for  $r_j$ . We can also obtain a composite  
 368 likelihood of our data under a neutral model ( $N$ ),  $\mathcal{L}_C(N; D_\ell)$ , which is only parameterized by  $\mathbf{F}$ . This  
 369 framework enables us to:

- 370 1. Identify the maximum likelihood location of the selected locus in a region by varying the location of the  
 371 proposed selected site. For a given region and model of convergent adaptation we vary the location of  
 372 the selected site, taking the maximum composite likelihood over a grid of parameters. We take as our  
 373 best estimate of the location under a given model of convergence, the maximum composite likelihood  
 374 location of the selected site ( $\hat{\ell} = \underset{\ell, \Theta_M}{\text{arg max}} \mathcal{L}_C(M, \Theta_M; D_\ell)$ ).
- 375 2. Determine the parameter(s) which maximize our composite likelihood estimates under a given model  
 376 at a given location of the selected site ( $\ell$ ). We obtain these maximum composite likelihood estimate  
 377 (MCLE) parameters by evaluating the composite likelihood across a grid of parameters for a given  
 378 location of the selected site ( $\hat{\Theta}_M = \underset{\Theta_M}{\text{arg max}} \mathcal{L}_C(M, \Theta_M; D_\ell)$ ).
- 379 3. Distinguish between modes of convergence, and neutrality, in a genomic region by comparing the  
 380 maximum likelihood under various models of convergent evolution. At a given location of the se-  
 381 lected site ( $\ell$ ) we compare the maximum composite likelihood of each model to the neutral model  
 382 ( $\log(\mathcal{L}_C(M, \hat{\Theta}_M; D_\ell) / \mathcal{L}_C(N; D_\ell))$ ).

383 This composite likelihood ignores the correlation in allele frequencies (linkage disequilibrium) between  
 384 neutral sites so the composite likelihood surface will be too peaked. A number of authors have taken  
 385 composite likelihood approaches to inferring a range of population genetic parameters (e.g. Hudson (2001);  
 386 see Larribe and Fearnhead (2011); Varin et al. (2011) for a broader statistical views on composite likelihood).  
 387 In the setting of inferring genome-wide parameters, e.g. parameters of neutral demographic models, the  
 388 maximum composite likelihood parameter estimates are known to be consistent in the limit of many unlinked  
 389 genomic regions (Wiuf, 2006). While in general composite likelihood methods perform well, in all of these  
 390 settings typical measures of uncertainty of parameters (confidence intervals) and model choice methods (e.g.  
 391 AIC) are undermined due to the over peakiness of the likelihood.

392 Composite likelihood approaches have also been used in the context of selective sweeps, starting with  
 393 Kim and Stephan (2002) who take a composite likelihood formed like Equation 17 of the product of marginal  
 394 probabilities of allele frequencies within a single population moving away from a proposed selected site (an  
 395 approach expanded on by Kim and Nielsen, 2004; Nielsen et al., 2005; Chen et al., 2010; DeGiorgio et al.,  
 396 2014; Racimo, 2016). Our method is most closely related to that of Chen et al. (2010) and Racimo (2016)  
 397 who look at allele frequencies across two or three populations respectively, and look for the signal of a sweep

398 in one of the populations (or in the case of Racimo, 2016, in the ancestor of a pair of populations). We note  
399 that we have a further layer of abstraction over these previous composite likelihood methods. Extending Kim  
400 and Stephan (2002), previous methods have calculated the likelihood of the sample frequency considering  
401 a binomial draw from some underlying population frequency, which is naturally modeled as being bounded  
402 between 0 and 1. We, however, use a multivariate normal likelihood to model our sample frequencies, which  
403 does not bound allele frequencies between 0 and 1. This further abstraction is justified by the fact that by  
404 using the multivariate normal approach we are able to handle arbitrarily large number of populations with  
405 arbitrary population structure and to flexibly model different forms of selection into an easily extendable  
406 form to the covariance matrix. Future work could potentially concentrate on hybrid approaches, combining  
407 the flexibility of our approach with the realism of previous approaches.

## 408 3.2 Inference method on simulated data

409 To test our method, we utilized the datasets generated using `mssel` (as discussed above with details in  
410 Appendix A.2) to see if we could recover the parameters and convergent mode used for simulation. The  
411 neutral coancestry matrix  $\mathbf{F}$  was estimated using data from 1000 runs with no selection (as described in  
412 Appendix A.1). We assume that the model parameters  $N_e$  and  $r$  are known and we set these at the values used  
413 to generate the simulations. We calculated the composite log-likelihoods for each of the simulated datasets  
414 under the following four models: neutral (no selection), independent sweep model, standing variation model,  
415 and migration model with the beneficial allele originating in population 2. We calculate the likelihoods  
416 under a dense grid of selection coefficients ( $s$ ), migration rates ( $m$ ), and standing times ( $t$ ). In the standing  
417 variation model, the standing frequency ( $g$ ) is held at 0.001. See Appendices A.2.4 and A.2.5 for details.  
418 We repeat this procedure for each of 100 runs of all simulated datasets. To compare between models, we  
419 calculate the composite log-likelihood differences between the true model and all other models including  
420 the neutral model, at the maximum composite likelihood parameter estimate (MCLE) obtained under each  
421 model.

### 422 3.2.1 Parameter estimation

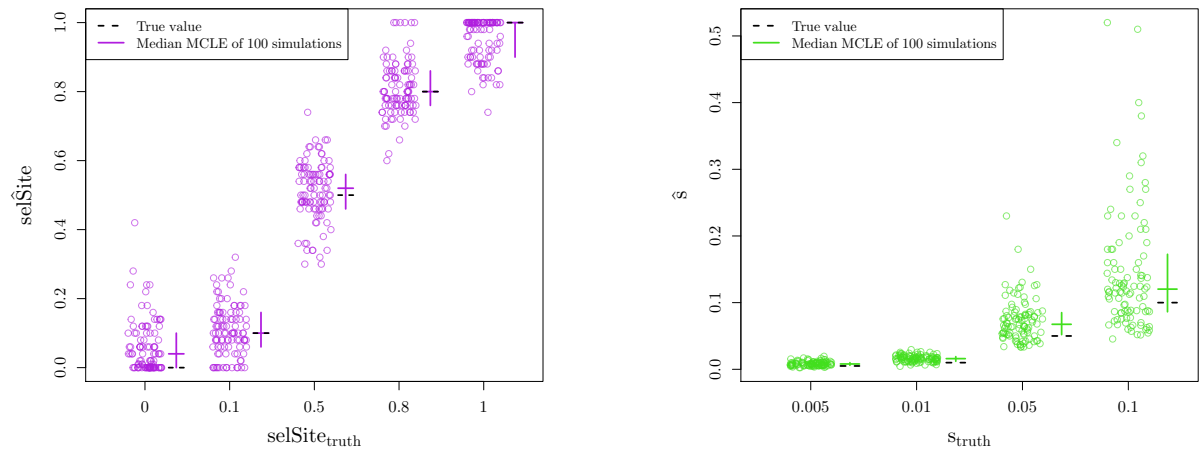
423 **Location of selected site** To explore our method's ability to localize the selected site, we vary the true  
424 location of the selected site simulating under the independent mutation model. We estimate the maximum  
425 composite likelihood location under the independent sweep model over a fine grid of locations and selection  
426 coefficients. The method is able to correctly identify the location of selection (Figure 4a), with higher  
427 accuracy when the true location of the site is in the middle of the window. The method does show an edge  
428 effect when the true location of the selected site is at the edge of the region of interest perhaps because we  
429 do not get to see the decay of coancestry on both sides of the selected site. Additionally, we are able to  
430 correctly estimate the strength of selection while allowing the location of the selected site to vary (Figure  
431 S1a) and there is no correlation between these joint parameter MLCEs (Figure S1b).

432 **Independent mutations model** To verify our ability to recover the selection coefficient, we simulated  
433 under the independent mutation model for a range of values for  $s$ , holding the location of the selected site  
434 at its true value. We are able to recover the parameters used for simulation (Figure 4b). The ability to  
435 correctly estimate  $s$  breaks down for large enough  $s$ , given a fixed window-size around the selected site and  
436  $r_{BP}$ , since we will not observe the full decay in coancestry.

437 **Standing variant model** To explore our inference using the standing variant model, we hold the location  
438 of the selected site at its true location and take as our estimate of  $s$  and  $t$  their values at the joint maximum  
439 composite likelihood. Under the standing variant model, we are again able to accurately estimate  $s$  (Figure  
440 S6). The inference of  $s$  and  $g$  simultaneously is somewhat more confounded (Figure 5). How the signal of  
441 the sweep within populations decays, as we move away from the selected site, is primarily determined by  $s$   
442 and  $g$  (see Equation 7). While a higher frequency of the standing variant ( $g$ ) can lead to a quicker decay,  
443 this can be partially compensated for the strength of the sweep being stronger (higher  $s$ , lower  $t_s$ ). This  
444 explains the  $J$ -shaped ridge in the likelihood surfaces for  $s$  and  $g$ , seen in Figure 5. Therefore, in practice  
445 we can often infer a lower bound  $s$  and an upper bound for  $g$ , but not find the precise values of each when

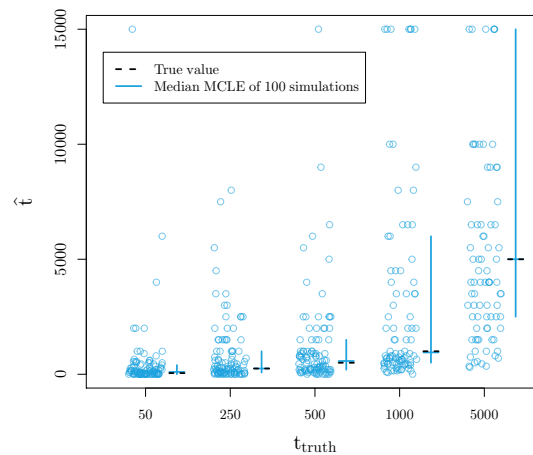
446 inference is performed under the standing variation model. We are able to accurately estimate the time the  
447 beneficial allele has been standing in the independent populations prior to selection,  $t$ , as shown in Figure  
448 4c. Our inference of  $t$  is relatively free of confounding with  $s$  and  $g$ , as  $t$  primarily governs the decays in  
449 coancestry between populations, making it separable from the scale of the sweep within populations.

450 **Migration model** We explored our inference under the migration model of parameters  $m$  and  $s$ , again  
451 fixing the location of the selected site and taking the joint maximum composite likelihood estimate. We are  
452 able to correctly estimate  $s$  (Figure S4b). However, we obtain poor estimates of the rate of migration,  $m$   
453 (Figure S4a). This is perhaps unsurprising as the coancestry coefficients under the migration model depend  
454 only weakly on  $m$ . We obtain fairly bimodal estimates of  $m$  that are usually either very low ( $10^{-5}$  to  $10^{-3}$ )  
455 or high (1). As the true value of  $m$  increases, we see fewer estimates of small  $m$  and more estimates of  $m = 1$ .  
456 These estimates of  $m$  seem to be a true reflection of the patterns in the simulated datasets. Specifically, this  
457 effect is mostly observed in the variance within the recipient population as Equation 12 depends on  $m$  in  
458 both  $Q$  and  $\delta$ . High  $m$  estimates correspond to datasets with lower empirical levels of coancestry within the  
459 recipient than datasets where low estimates of  $m$  were obtained (Figure S5). We believe that the bimodality  
460 results from stochasticity in how many lineages ancestral to the sample migrate before they recombine off the  
461 sweep in the recipient population. While our estimates of  $m$  are noisy, the migration model does capture  
462 key features of the spread of adaptive alleles by migration, allowing it potentially to be distinguished from  
463 other modes of convergence. We now turn to the performance of the method in distinguishing modes of  
464 convergence.



(a) MCLE of the **location of selected site** for 100 simulations under the **independent mutation model** (10 chromosomes per population,  $N_e = 100,000$ ,  $s = 0.05$ )

(b) MCLE of the **strength of selection ( $s$ )** for 100 simulations under the **independent mutation model** (10 chromosomes per population,  $N_e = 100,000$ )



(c) MCLE of the **standing time ( $t$ )** for 100 simulations under the **standing variant model** (10 chromosomes per population,  $N_e = 10,000$ ,  $s = 0.01$ ,  $g = 0.001$ ). For scale, we left out estimates of  $t > 15,000$  (2, 9, and 21 data points when  $t_{\text{truth}} = 500$ , 1000, and 5000, respectively.)

Figure 4: Maximum composite likelihood **parameter estimates** calculated under **model used for simulation**. We vary the true value of the parameter used for simulations along the x-axis and show the MCLE for each of 100 simulations (points). Crossbars indicate first and third quartiles with second quartiles (medians) as the horizontal line. The true values of the parameters are marked with dashed, black lines.

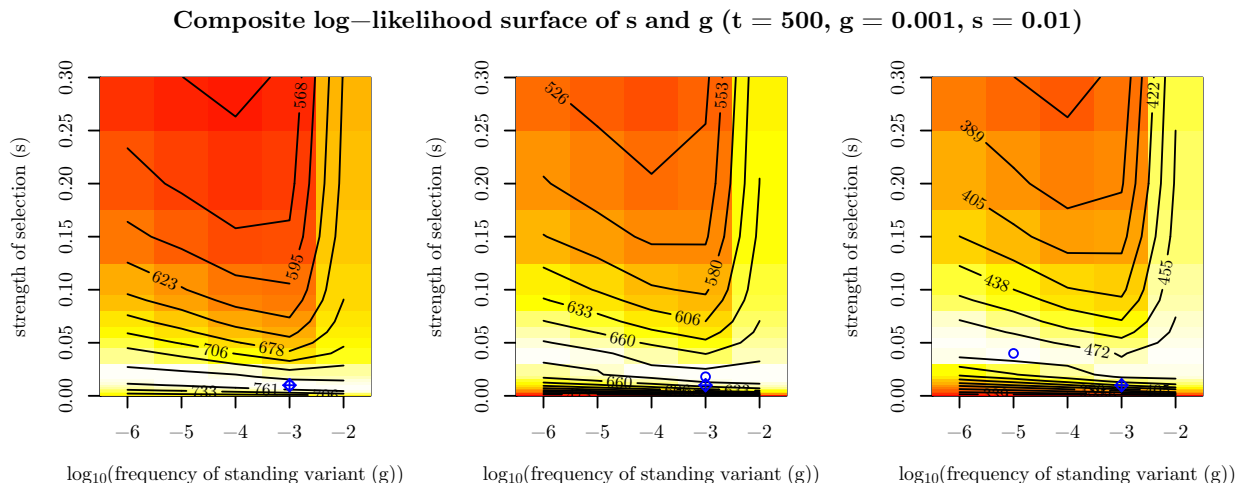


Figure 5: Composite log-likelihood surface of the **strength of selection** ( $s$ ) and the **frequency of standing variant** ( $g$ ) for three simulations (with  $N_e = 10,000$ ,  $t = 500$ ,  $g = 0.001$ ,  $s = 0.01$ ) to exemplify confounding of  $s$  and  $g$  under the **standing variant model**. Blue diamond pluses represent the true location of the parameters used for simulation. Blue circles represent MCLE.

### 465 3.2.2 Model comparison

466 To test the ability of our method to distinguish between modes of convergence, we calculated the maximum  
 467 composite log-likelihood of 100 simulations for each dataset generated under both the true model and all  
 468 other models with a fixed, fine grid of parameter values. The location of the selected site is fixed at its true  
 469 location. The results are summarized in Figure 6, which shows histograms of the difference in maximum  
 470 composite log-likelihoods calculated under a given model relative to the true model used for simulation. For  
 471 example, in evaluating the independent mutations model, we present the difference in the composite log-  
 472 likelihoods calculated for data simulated under the independent mutations model for all other models and  
 473 the composite log-likelihood calculated for the true independent mutations model. Thus, values less than  
 474 zero indicate that the correct model has a higher maximum composite log-likelihood than the true model.  
 475 Conversely, values greater than zero indicate the incorrect model of convergence has a higher composite  
 476 log-likelihood than the true model. For inference under the migration model, we fix the source to be the  
 477 true source of the selected allele when simulating under the migration model, and to an arbitrary one of the  
 478 two selected populations when performing inference on simulations under other models.

479 **Neutral model** We first compare the composite likelihoods calculated for data generated with no selection.  
 480 For the selection models, we fix the location of the selected site. The distributions of the resulting composite  
 481 log-likelihood ratios are shown in Figure 6a. As expected for a composite likelihood, the composite log-  
 482 likelihood ratio between a convergent selection model and the neutral model with no selection are inflated  
 483 compared to those expected under the usual asymptotic  $\chi^2$  distribution. However, these likelihood ratio  
 484 differences are relatively small compared to those we observed when simulating under alternative models.  
 485 This is because when  $s \rightarrow 0$  in all models with selection, the coancestries converge to our neutral expectations.  
 486 Indeed when we look at the MCLE for the strength of selection ( $\hat{s}$ ) under the incorrect models with selection,  
 487 we see that for all nearly simulations  $\hat{s}$  is close to zero 0 (Figure 7a). Overall, this suggests that our null  
 488 model is reasonably well calibrated, given the limitations of composite likelihood schemes.

489 **Independent mutations model** As shown in Figure 6b, we are able to correctly distinguish between  
 490 a neutral model of no selection and the true independent mutation model by at least 160 composite log-  
 491 likelihood units even for relatively weak selection ( $s = 0.005$ ). This difference increases as the true value of  
 492  $s$  increases. This same relationship is true when comparing the migration model to the true independent

493 mutation model. Therefore, we have good ability to distinguish the independent sweeps model from neutral  
494 and migration model over a range of selection coefficients.

495 Our ability to distinguish between the standing variation model and the true independent mutation model  
496 is less clear. When the true  $s$  is small, the two models have comparable composite log-likelihoods, with  
497 differences ranging from -3 to 20. This difference decreases, with higher likelihood for the true independent  
498 mutation model more frequently, as  $s$  increases. This result makes sense when we look into the maximum  
499 likelihood estimate of the parameter  $t$  (Figure 7b). We obtain estimates of  $t$  approaching our highest  
500 value on the grid ( $10^6$ ). Thus, we may not be able to distinguish between the cases where the origins of  
501 the beneficial allele are truly independent or whether selection has been on a single variant that has been  
502 standing independently for a long time as these two models converge for large  $t$ .

503 **Standing variant model** Simulating under the standing variation model, the picture is more complicated.  
504 Like the other models, we can exclude the neutral model, although note that this would become challenging  
505 when the allele has been standing at high frequencies,  $g \gg 0$  (Berg and Coop, 2015). When the independent  
506 standing time,  $t$ , is small, we see little difference in the composite log-likelihoods between the true standing  
507 model and the migration model. As  $t$  increases, we see a larger difference between these two models. However,  
508 as  $t$  increases, the composite log-likelihood difference between the independent mutation model and standing  
509 variation model tightens around 0. These results fit our expectations as we know the models look similar  
510 in the extreme values of  $t$ , the migration model when the standing time is small and independent mutation  
511 model when the standing time is large, respectively.

512 **Migration model** We are able to distinguish the migration model from the neutral and independent  
513 sweeps model. However, the standing variation and true migration model are again somewhat confounded.  
514 The values of the composite log-likelihood differences range from -44 to 123 when  $m = 10^{-4}$  and this range  
515 narrows closer to 0 as  $m$  increases. These results fit our understanding when we again look at the MCLEs  
516 of  $t$  in the standing model. Now, the estimates are at  $t = 0$  (Figure 7c) indicating it is hard to distinguish  
517 between convergence that is due to migration or selection on a shared standing variant that has only been  
518 standing for a very short time, as they result in similar patterns in decay of coancestries.

519 **Summary** We can clearly distinguish the outcomes of the migration and independent sweeps models from  
520 each other. Both models are hard to distinguish from the standing variation case, but in very different  
521 regimes of the standing variation model. The estimated time the variant has been standing ( $t$ ) for is a  
522 helpful indicator of the mode of convergence, with very low estimates meaning that the standing model  
523 is indistinguishable from the migration model, while very high estimates mean that the standing model is  
524 indistinguishable from the independent sweeps model. When data is simulated under the standing model  
525 with intermediate values of  $t$ , we can distinguish this from both independent sweeps and recent migration  
526 models. This is because an intermediate value of  $t$  generates a covariance pattern not well explained by either  
527 other model. Therefore, while comparing the maximum composite likelihoods between models is useful, the  
528 estimated value of  $t$  is useful in judging the different models.



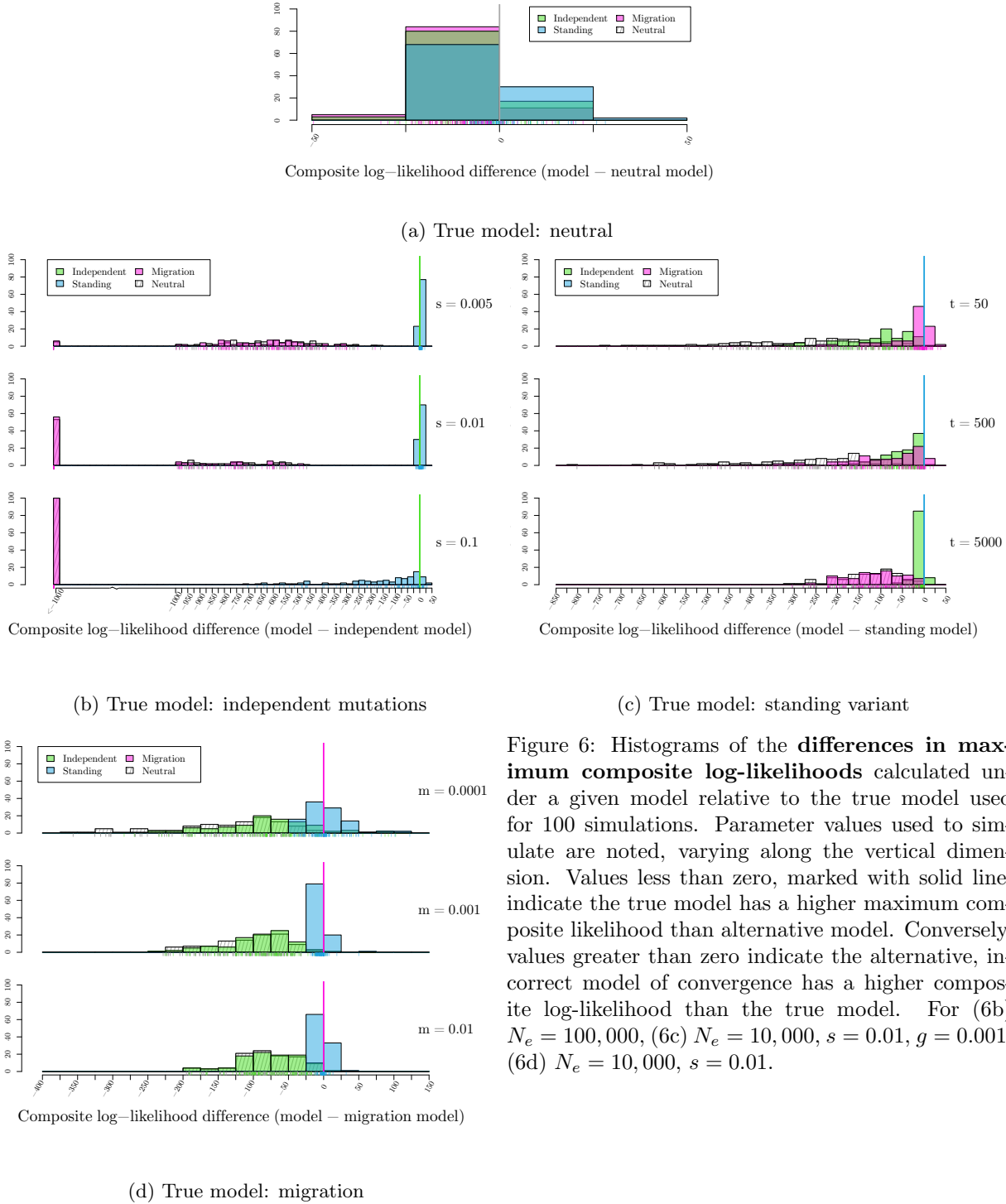
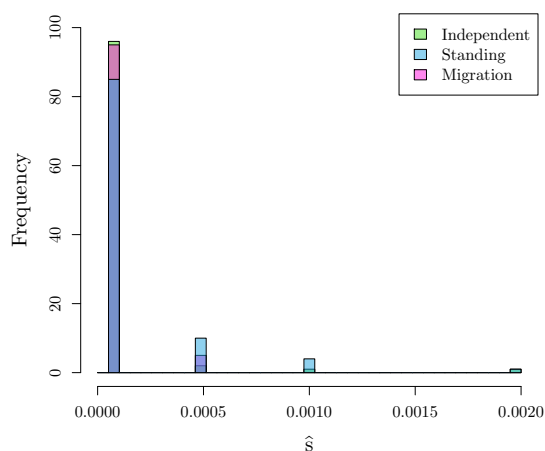
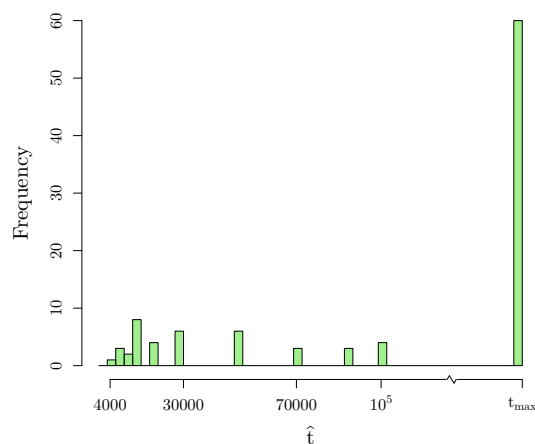


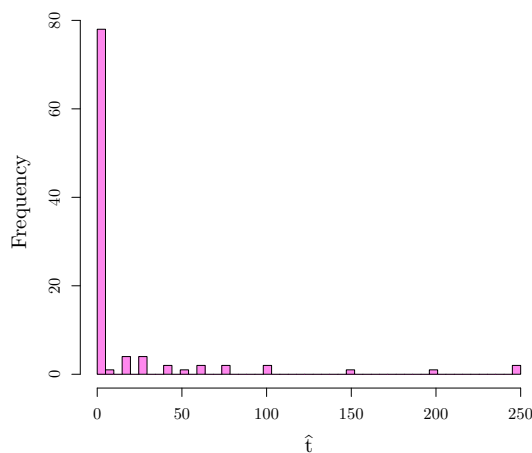
Figure 6: Histograms of the **differences in maximum composite log-likelihoods** calculated under a given model relative to the true model used for 100 simulations. Parameter values used to simulate are noted, varying along the vertical dimension. Values less than zero, marked with solid line, indicate the true model has a higher maximum composite likelihood than alternative model. Conversely, values greater than zero indicate the alternative, incorrect model of convergence has a higher composite log-likelihood than the true model. For (6b)  $N_e = 100,000$ , (6c)  $N_e = 10,000$ ,  $s = 0.01$ ,  $g = 0.001$ , (6d)  $N_e = 10,000$ ,  $s = 0.01$ .



(a) Histogram of MLE of the **strength of selection ( $s$ )** under all convergent models where the **neutral model is true model** used for simulations.



(b) Histogram of MLE of the **standing time ( $t$ )** under standing variant model where the **independent mutation model** is true model used for simulations ( $s = 0.01$ ,  $N_e = 100,000$ ).



(c) Histogram of MLE of the **standing time ( $t$ )** under standing variant model where the **migration model is true model** used for simulations ( $m = 0.001$ ,  $s = 0.01$ ,  $N_e = 10,000$ ).

Figure 7: Histograms of MLE for **parameters** estimated under **incorrect models**.

## 529 4 Applications

### 530 4.1 Copper tolerance in *Mimulus guttatus*

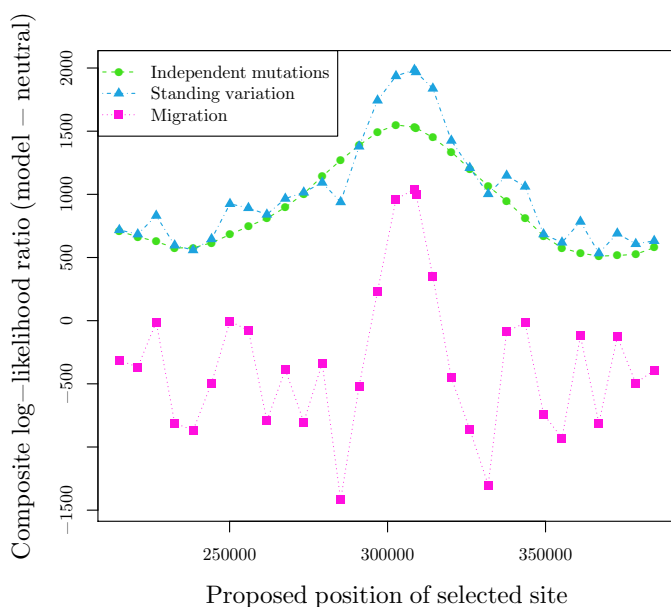
531 The study of adaptation to toxic mine tailings is a classic case of rapid local adaptation to human altered  
 532 environments (MacNair et al., 1993). We apply our inference method to investigate the basis of the convergent  
 533 adaptation seen between populations of the annual wildflower *Mimulus guttatus* to copper contaminated soils  
 534 near Copperopolis, CA. Wright et al. (2015) sequenced pooled samples from 20-31 individuals from two mine  
 535 and two off-mine populations from two distinct copper mines in close geographic proximity (all populations  
 536 within 15 km of each other) to 34-72X genome-wide coverage for each population. They observed elevated

537 genome-wide estimates of genetic differentiation between mine and off-mine populations ( $F_{ST}$  M/OM= 0.07  
538 and 0.14), with similar levels of differentiation between the mine populations ( $F_{ST}$  MM= 0.13). Only a small  
539 number of regions had high levels of differentiation. Here, we focus on the region with the strongest signature  
540 of differentiation between the two mine/off-mine pairs found on Scaffold8 by Wright et al. (2015). They  
541 observed low genetic diversity within each mine population in this region compared to off-mine populations.  
542 When the mine populations are compared to each other, they have elevated differentiation in this region,  
543 except for in the center where they share a nearly identical core haplotype. This pattern suggests the sweeps  
544 may not have been independent within each mine population, and that the sweep is possibly shared either  
545 due to migration or selection of shared standing variation.

546 We estimate the  $\mathbf{F}$  matrix using SNPs from twelve scaffolds that showed no strong signals of selection  
547 (shown in Table S6). Using all SNPs in the 169.3 kb Scaffold8, we apply our inference framework to both  
548 identify the locus under selection and distinguish between modes of convergence between the two mine  
549 populations. We move the proposed selected site along this scaffold and calculate the composite likelihood  
550 under our three modes of convergent adaptation: (1) both mine populations have had independent mutations  
551 at the same locus, (2) the beneficial allele was standing in the ancestor of the two mine populations and  
552 selection occurred independently once the mine populations were isolated, and (3) the beneficial allele arose  
553 in one of the mine populations and spread to the other via migration. We estimate the maximum composite  
554 likelihood over a dense grid of parameters used to specify these models (Table S7). For the migration model,  
555 we allow both adapted populations to be possible sources. We use an  $N_e = 7.5 \times 10^5$ , calculated from the  
556 observed pairwise diversity  $\pi = 4N_e\mu$  using a mutation rate of  $\mu = 1.5 \times 10^{-8}$  and  $r_{BP} = 4.72 \times 10^{-8}$  (Lee,  
557 2009).

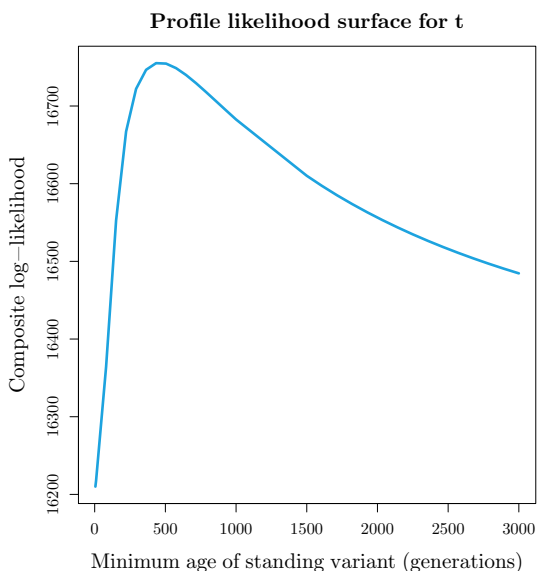
558 In Figure 8a, we summarize the results, showing the difference in maximum composite log-likelihoods  
559 between a given model of convergence and the neutral model of no selection as a function of the proposed  
560 selected sites along the scaffold. We see the three likelihoods peaking when the selected site is approximately  
561 at position 302665-308504 and that the model with the highest likelihood is selection on shared ancestral  
562 standing variation. Focusing on this model at the most likely selected site, we can obtain parameter estimates  
563 for the strength of selection ( $s$ ), standing frequency of the beneficial allele ( $g$ ), and the amount of time that  
564 the beneficial allele has been standing in both mine populations after they have been isolated but prior to  
565 selection ( $t$ ). This time also has the interpretation of the minimum age of the standing variant as it has  
566 been standing for at least this amount of time and potentially longer in the ancestral population. We see the  
567 maximum composite log-likelihood is obtained when this time is approximately 430 generations (Figure 8b).  
568 As copper mining started in 1861 in this region (Aubury 1908), this suggests the tolerance allele was present  
569 prior to the onset of mining. The strength of selection and starting frequency of the allele are confounded  
570 (Figure 8c) as expected. Our maximum composite log-likelihood parameter estimates suggest selection was  
571 relatively strong ( $>0.02$ ) and the allele was not standing at very high frequencies ( $< 10^{-3}$ ) when selection  
572 began.

573 We also ran the standing variation model with one of the two copper-mines as the source (as detailed in  
574 Appendix A.3). The standing variant likelihood surfaces, over selected sites, using either copper population  
575 were identical to the case of the standing variant model with no source (see Figure S7a). Therefore, there is  
576 little information about the source of the standing variant. This is perhaps unsurprising as there is relatively  
577 little hierarchical structure among the populations. The composite maximum likelihood estimate of  $t$  is  
578 higher for the models of standing variation with a source, than the simple model of standing variation (see  
579 Figure S7b). This is likely because making one of the populations a source of the standing variant increases  
580 the covariance around the selected site among the selected populations, as described in Appendix A.3, and  
581 so the model compensates by increasing the rate of decay of this covariance.

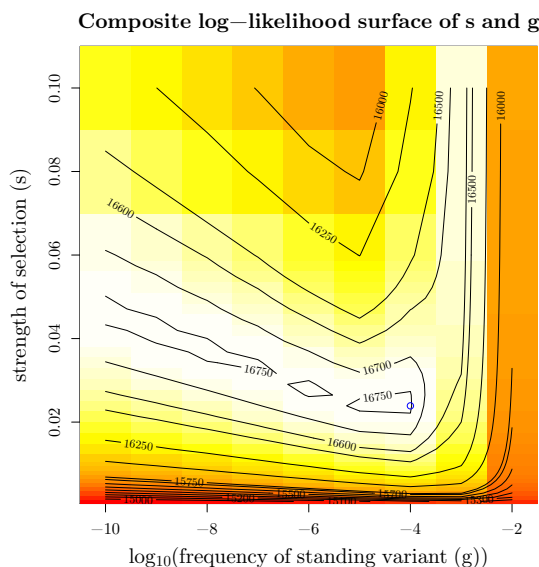


(a)

Figure 8: **Inference results for *Mimulus guttatus* copper tolerance adaptation on Scaffold8.** (a) Composite log-likelihood ratio of given model relative to neutral model of no selection as a function of the proposed selected site. (b, c) MCLE of parameters in standing variation model with position 308503 as selected site. (b) Profile composite log-likelihood surface for minimum age of standing variant, maximizing over other parameters, with peak at 430 generations (c) Composite log-likelihood surface for strength of selection versus frequency of standing variant. Blue circles represents point estimate of joint MCLE ( $\hat{s} = 0.024$ ,  $\hat{g} = 10^{-4}$ ).  $t$  is held constant at MCLE of 430 generations.



(b)



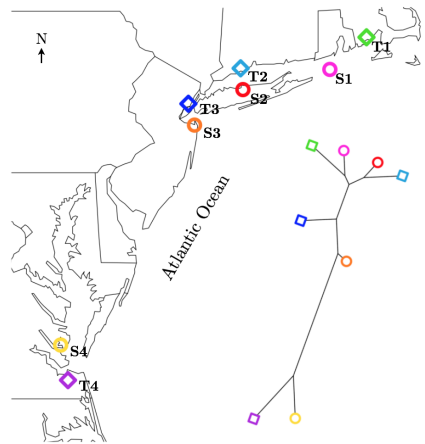
(c)

## 582 4.2 Industrial pollutant tolerance in *Fundulus heteroclitus*

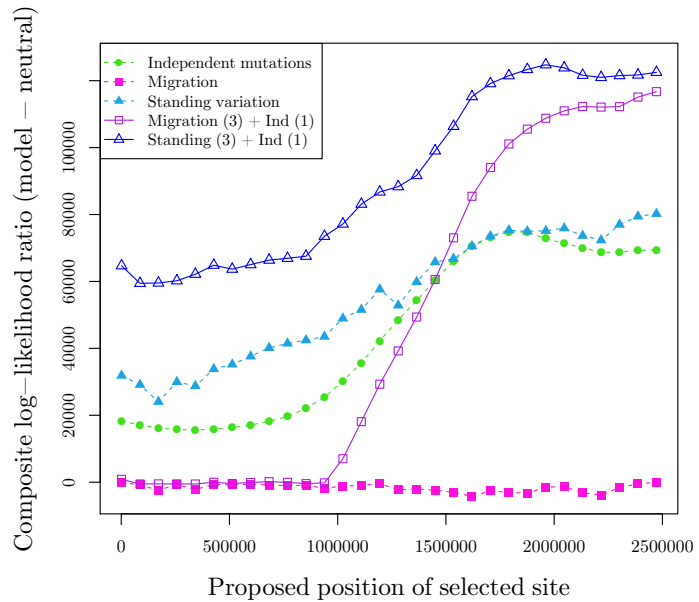
583 We demonstrate how our method can be extended to more complex population scenarios. Populations of  
 584 the Atlantic killifish, *Fundulus heteroclitus*, have repeatedly adapted to typically lethal levels of industrial  
 585 pollutants (Nacci et al., 1999, 2010). Reid et al. (2016) have sequenced 43-50 individuals from four pairs of  
 586 pollutant-tolerant and sensitive populations along the U.S. Atlantic coast (see Figure 9a), sequencing each  
 587 individual to 0.6-7X depth. The southern pair of populations form a distinct clade relative to the northern  
 588 populations, consistent with a phylogeographic break centered on New Jersey (Duvernell et al., 2008).

589 Reid et al. (2016) found that a number of the strongest signals of recent selection are shared between all  
590 tolerant populations, suggesting genotypic convergent adaptation. We focus our method on their strongest  
591 signal of selection, Scaffold9893 (GPS\_009145616.1, the scaffold containing the AIP gene), where all four pairs  
592 of tolerant/sensitive populations sampled show high levels of differentiation. Here, we test the hypotheses  
593 that all four tolerant populations show convergent adaptation due to our three previous modes of independent  
594 mutation, migration, or selection on shared ancestral variation. For our standing variation model, we specified  
595 the source of the standing variant (as described in Appendix A.3). We also test the hypotheses that there  
596 is an independent mutation in the southern tolerant population while the three northern populations are  
597 sharing a sweep at this locus, either due to migration between populations or selection on variation present  
598 in the ancestor of the Northern populations. This latter set of hypotheses is consistent with the fact that  
599 Reid et al. (2016) detect a shared haplotype in the three northern tolerant populations while a different  
600 haplotype appears to have swept in the southern tolerant population. We estimated the  $\mathbf{F}$  matrix from four  
601 scaffolds that show no strong signal of selection, and it is shown in Table S8. We use  $N_e = 8.3 \times 10^6$  and  
602  $r_{BP} = 2.17 \times 10^{-8}$  (N. Reid personal communication).

603 The results are summarized in 9b. For the models where all four tolerant populations share the selected  
604 allele by either migration or standing variation, we plot the maximum composite log-likelihood for the most  
605 likely source at each location of the selected site (to reduce the number of lines plotted, see Figure S8 for  
606 the full figure). We see the model with the highest composite log-likelihood is when convergence is due to  
607 selection on shared standing variation in the North and an independent mutation in the southern tolerant  
608 population. This occurs when the selected site is at approximately position 1960000 on the scaffold. This  
609 model has the highest composite log-likelihood when the source population of the standing variant is T3,  
610 southernmost population sampled in the North (composite log-likelihood = 547060), but this model may not  
611 be distinguishable from that where the source is T2 (545580). Under this model, we obtain the maximum  
612 composite log-likelihood estimate of the minimum age of the standing variant,  $t$ , of eight generations (Figure  
613 10a). This implies the beneficial allele has been standing for a negligible time independently in the northern  
614 populations prior to selection or that migration is assisting the spread of this allele as both scenarios lead  
615 to similar decays in shared coancestry as we move away from the selected site. Lastly, again, we see partial  
616 confounding of the strength of selection and the frequency of the standing variant (Figure 10b) but our  
617 results indicate selection has been very strong ( $>0.3$ ) and the allele was initially at a very low frequency  
618 ( $< 10^{-6}$ ).

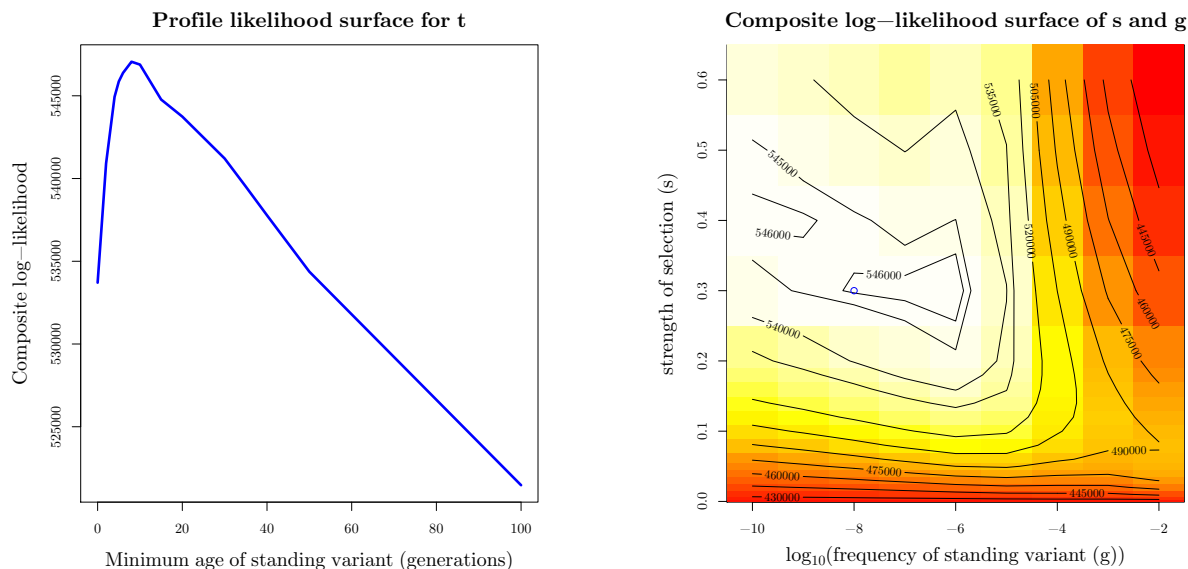


(a) Map of sampled killifish populations with phylogenetic tree, showing that the southern pair (T4, S4) are more distant than other populations. Tree is estimated from genome-wide biallelic SNP frequencies using Phylogeny Inference Package (PHYLIP) Gene Frequencies and Continuous Characters Maximum Likelihood (CONTML) module (see Reid et al. (2016) for more information).



(b) Composite log-likelihood ratio of given model relative to neutral model of no selection as a function of the proposed selected site. Closed points represent models where all four populations have same convergent mode while open points represent Southern population (T4) having an independent mutation at the proposed selected site. We show likelihoods maximizing over possible sources, but all results can be seen in Figure S8.

Figure 9: Inference results for *Fundulus heteroclitus* pollutant tolerance adaptation on Scaffold9893



(a) Profile composite log-likelihood surface for minimum age of standing variant, maximizing over other parameters, showing the beneficial allele has been standing for a very short amount of time in our three northern populations (8 generations).

(b) Composite log-likelihood surface for strength of selection versus frequency of standing variant. Blue circle represents point estimate of joint MLE ( $\hat{s} = 0.3$ ,  $\hat{g} = 10^{-8}$ ).  $t$  is held at MLE of 8 generations.

Figure 10: The composite likelihood surfaces for the parameters for *Fundulus heteroclitus* convergent data in combined standing variation and independent sweep model with position 1961198 on Scaffold9893 as selected site and population T3 as source.

## 5 Discussion

In this paper we have presented a novel approach to identify the loci involved in convergent adaptation and to distinguish among the three ways genotypic convergence can arise: selection on (1) independent mutations, (2) standing variation present in the ancestor of the selected populations, and (3) beneficial alleles introduced via migration. We leverage the effects selection has on linked neutral sites via a coalescent-based model approach that captures many of the heuristics that have been used in previous studies. This approach also allow us to potentially distinguish between more subtle models, such as the origin and the direction of gene flow of a beneficial allele, since they are explicitly modeled in our framework. Our approach takes advantage of information among all of the population samples simultaneously while accounting for population structure. Therefore, it naturally accommodates information from across multiple samples, rather than just pairs of populations, and thus offers a number of advantages in identifying the mode of convergence over other approaches. We provide the relevant R code for our approach in <https://github.com/kristinmlee/dmc>.

**Distinguishing among models** We have demonstrated that our method is able to accurately distinguish among modes of convergent adaptation, across a relatively wide parameter space, in simulated data. However, we do see some confounding of models in particular regions of parameter space. In particular, we see the patterns generated from a model of selection on ancestral standing variation can look like our expectations for the other two modes of convergent adaptation for extreme values of the parameter  $t$ , the time the beneficial allele has been standing time independent in the selected populations. When  $t$  is small, we see confounding between the standing model and a model of convergence due to gene flow. The two models are very similar since in our standing variation model, as  $t \rightarrow 0$ , the covariance in the deviations of a neutral allele between selected populations approaches the variance within a selected population (the strong overlap in models is especially true when we have a source for the standing variant). Intuitively this indicates that the beneficial

642 allele is on a haplotype that is mostly shared among the selected populations. This can be due to a very  
643 young standing variant shared amongst very closely-related populations from an ancestral population, a  
644 standing variant that was shared by gene flow before selection, or by the selected haplotype quickly moving  
645 across populations by gene flow after selection began (which are all closely related models, see Welch and  
646 Jiggins, 2014, for additional discussion).

647 To illustrate distinguishing between these possibilities we now revisit our applications. The Northern  
648 tolerant killifish populations, under a standing variation model, have a very low estimate of  $t$ . We can likely  
649 rule out the sweep occurring in an ancestor of the tolerant Northern populations, as both T1 and T2 are sister  
650 populations to different sensitive populations. We note that in cases where two populations that are sister  
651 share a sweep, we can extend our models to test if the sweep is ancestral or truly convergent. Furthermore,  
652 given the very low estimate of  $t$  the allele cannot have been standing since the common ancestral population  
653 of T1, T2, T3. Therefore, the allele must be shared by gene flow among the three populations and it seems  
654 likely that the migration of the allele occurred either after selection began in one of the populations or very  
655 shortly before. Interestingly, however, they find no other signals of admixture from migration elsewhere in the  
656 genome between Northern tolerant populations. The case for adaptation from ancestral standing variation  
657 is clearer for the *Mimulus* copper tolerance example. Here, the estimate of  $t$  is much greater than zero and  
658 indeed older than the putative selection pressure. Additionally, the standing variant model considerably  
659 outperforms the migration model (Figure 8a). That said, given that the level of neutral differentiation of the  
660 mine populations very likely reflects much more than 430 generations of drift, it seems likely that this allele  
661 is shared between the mine populations by gene flow but that the allele was standing in both populations for  
662 some time before selection began (as described by the standing model with a source model, see Appendix  
663 A.3 and Figure Figure S7a). Thus, distinguishing among these models is possible in some cases, but may  
664 require extra knowledge of population history.

665 Conversely, when  $t$  is large, we see a collapse of our standing model onto a model of convergence due to  
666 independent mutations in our selected populations. This intuition holds forwards in time since as  $t \rightarrow \infty$   
667 generations, recombination in our isolated populations independently breaks down the similarity of the  
668 haplotypes carrying the beneficial mutation. Thus, when selection for the standing variant begins, even  
669 tightly-linked, hitchhiking neutral alleles will not be shared between populations more than expected by  
670 chance. This is also the case when beneficial alleles arise multiple times independently. For example, in the  
671 case of the killifish, it is formally possible that the signal of independent selection in the Southern tolerant  
672 population is actually due to a very old standing variant shared with the Northern populations where there  
673 is almost no overlap between the Southern and Northern tolerant populations in the haplotype the selected  
674 allele is present on, even close to the selected site. As the precise functional variant(s) in this swept region are  
675 currently unknown (Reid et al., 2016) it is hard to totally rule out this very old standing variant hypothesis.  
676 In other cases it may be possible to rule out the standing variant hypothesis with very large parameter  
677 estimates of  $t$  if we know more about the population histories (i.e. our selected populations split more  
678 recently than the standing time). Additionally, it may be possible to totally rule out the standing variant  
679 hypothesis in cases where if the functional variants can be tracked down to clearly independent genetic  
680 changes (e.g. Tishkoff et al., 2007). However that degree of certainty may be difficult to achieve in many  
681 cases.

682 **Extendibility and flexibility of our approach** We show the applicability of our method on two em-  
683 pirical examples of convergent adaptation: the evolution of copper tolerance in *Mimulus guttatus* and of  
684 pollutant tolerance in *Fundulus heteroclitus*. The latter exemplifies the extendibility and flexibility of our  
685 approach. As the number of selected populations increase, our potential number of hypotheses grows since  
686 any grouping of two or more populations could share selection due to migration or standing variation. Ad-  
687 ditionally, with more populations, we have more potential sources of the beneficial allele in the migration  
688 model. Our model could also be extended to have selection occurring in some of the adapted populations  
689 and the neutral model in others, to identify genomic regions that are not experiencing convergent adaptation  
690 among all populations sharing the selected environment. These models are all relatively easy to implement  
691 into our framework; however, the sheer number of possible hypotheses as the number of populations grows  
692 will likely call for some more systematic way of implementing these models and exploring their relationships.



693 **Caveats and possible extensions** Studying repeated evolution has long played a key role in evolutionary  
694 biology as a tool to help identify the ecological and molecular basis of adaptation. It is worth noting with  
695 this approach, we are able to identify sweeps in the same region and whether they appear to be shared or  
696 independent. However, in the scale of an entire genome, it may be possible for two, unrelated sweeps to  
697 overlap. In the case of adaptation via independent mutations across multiple populations, it is especially  
698 hard to determine whether selection at the same site was acting on the same phenotype. It is potentially  
699 more plausible to claim that the phenotype and selection pressure are shared among populations in cases  
700 where the swept haplotype is shared. Ultimately, in demonstrating convergence, we will have to rely on  
701 a range of evidence. Shared sweeps can offer one substantial piece of evidence, particularly when we are  
702 studying recent adaptation to a strong selective pressure that is distinct to the adapted populations.

703 We assume a single selected change underlies the sweep within a population, and that recombination is  
704 free to break down associations between neutral alleles and this selected variant. If, for instance, selection  
705 acts on an epistatic, haplotypic combination of allele that sweeps, a long haplotype could be shared between  
706 populations not due to recent migration but because selection acts against recombinants breaking up the  
707 haplotype (Kelly and Wade, 2000). Convergent adaptations due to shared inversions also violate the as-  
708 sumptions of our method. Inversions can repress recombination across the entire inversion (see Kirkpatrick,  
709 2010, for a recent review). Inversions significantly alter both neutral and selective model expectations (e.g.  
710 Guerrero et al., 2012) and could lead to long shared haplotypes among populations even if the shared inver-  
711 sion is old. It may be possible to use our approach to model the decay in coancestries outside of the inverted  
712 region, but this requires knowledge of the inversion and its break points *a priori* and a detailed knowledge  
713 of recombination rates surrounding the inversion.

714 Additionally, our framework could be extended in various ways to both leverage more information and  
715 model more biologically relevant or interesting scenarios. There is more information to be gained from  
716 haplotypes and associations between sites that we fail to include in our composite likelihood when we sum  
717 across information from individual sites. Additionally, models of migration that include selection against  
718 maladaptive migrants (Barton and Bengtsson, 1986; Charlesworth et al., 1997; Roesti et al., 2014) will be  
719 important to consider.

720 Finally, here we use this approach to analyze genomic regions that we *a priori* assume to be under  
721 convergent selection. We are currently working on ways to efficiently extend this approach to the application  
722 of genome-wide data to scan for genomic regions exhibiting convergence.

723 **Final thoughts** With the falling cost of population genomic sequencing, it is increasingly easier to obtain  
724 genome-wide polymorphism data from across many populations showing an adaptation to the same selective  
725 pressure. We hope that with the advent of these data in a wide range of systems and methods like those  
726 outlined here, we can gain insights into fundamental questions regarding the nature of adaptation and  
727 convergence.

## 728 6 Acknowledgements

729 We wish to thank members of the Coop lab for helpful discussion and feedback on earlier drafts. We'd also  
730 like to gratefully acknowledge Noah Reid, Andrew Whitehead, John Willis, and Kevin Wright sharing their  
731 data and thoughtful comments. This work was supported by the NSF GRFP awarded to K. Lee (1148897)  
732 and by grants from the National Science Foundation under Grant No. 1353380 to John Willis and G. Coop  
733 and the National Institute of General Medical Sciences of the National Institutes of Health under award  
734 numbers NIH R01 GM108779 awarded to G. Coop.

## 735 A Appendix

### 736 A.1 Coalescent interpretation of covariances and F-matrix estimation

Let  $x_{il}$  be the allele frequency of allele 1 in population  $i$  at locus  $l$ , and that the frequency of this allele in the ancestral population is  $\epsilon_l$ . Consider the covariance  $\text{Cov}(\Delta x_{il}, \Delta x_{jl})$  over replicates of the drift processes at locus  $l$ . We can write

$$\text{Cov}[x_{il}\epsilon_l, (x_{il} - \epsilon_l)] = \mathbb{E}[(x_{il} - \epsilon_l)(x_{jl} - \epsilon_l)] \quad (\text{A.1})$$

$$= \mathbb{E}[x_{il}x_{jl}] - \epsilon_l^2 \quad (\text{A.2})$$

737 which follows from the fact that  $\mathbb{E}[x_{il}] = \mathbb{E}[x_{jl}] = \epsilon_l$ . We can interpret  $\mathbb{E}[x_{il}x_{jl}]$  as the probability that we  
 738 sample a single allele in  $i$  and an allele in  $j$  and that they both are of type 1. Taking that interpretation,  
 739 assuming that there is no mutation,  $\mathbb{E}[x_{il}x_{jl}]$  is the probability that, tracing back a coalescent lineage from  
 740  $i$  and a lineage from  $j$ , both lineages trace back to type 1 alleles in the ancestral population. Let our pair  
 741 of lineages drawn from  $i$  and  $j$  coalesce with probability  $f_{ij}$ . If our lineages coalesce before reaching the  
 742 ancestral population then they will be identical by descent, and share the ancestral choice of allele. Therefore,  
 743 we can write

$$\mathbb{E}[x_{il}x_{jl}] = (1 - f_{ij})\epsilon_l^2 + f_{ij}\epsilon_l \quad (\text{A.3})$$

744 Then we can rewrite the covariance

$$\text{Cov}(\Delta x_{il}, \Delta x_{jl}) = f_{ij}\epsilon_l(1 - \epsilon_l), \quad (\text{A.4})$$

745 and for the variance we set  $i = j$ . Thus, under a model of genetic drift alone, we can interpret the entries of  
 746 our covariance matrix as expressions of the underlying coalescent probabilities.

747 **Estimating F** In the main text we assume that we have estimates of our neutral coancestry matrix **F**. We  
 748 now describe how we obtain these. From above, Equation A.3, the expectation of  $x_{il}x_{jl}$  across loci is

$$\mathbb{E}_l[x_{il}x_{jl}] = \mathbb{E}_l[(1 - f_{ij})\epsilon_l^2 + f_{ij}\epsilon_l] \quad (\text{A.5})$$

749 Therefore we can write estimate  $f_{ij}$  as

$$f_{ij} = \frac{\mathbb{E}_l[x_{il}x_{jl}] - \mathbb{E}_l[\epsilon_l^2]}{\mathbb{E}_l[\epsilon_l(1 - \epsilon_l)]} \quad (\text{A.6})$$

750 We can obtain an unbiased estimate of  $\mathbb{E}_l[\epsilon_l^2]$  and  $\mathbb{E}_l[\epsilon_l(1 - \epsilon_l)]$  using the sample allele frequencies from two  
 751 populations on either side of the root of the population phylogeny (see Supplement of Lipson et al., 2013).  
 752 Let  $i'$  and  $j'$  be a pair of populations that span the root of the population tree, then we can use the estimate

$$\mathbb{E}_l[\epsilon_l(1 - \epsilon_l)] = \mathbb{E}_l\left[\frac{1}{2}x_{i'l}(1 - x_{j'l}) + \frac{1}{2}(1 - x_{i'l})(x_{j'l})\right] \quad (\text{A.7})$$

753 Likewise, we use the estimate

$$\mathbb{E}_l[\epsilon_l^2] = \mathbb{E}_l\left[\frac{1}{2}x_{i'l}(x_{j'l}) + \frac{1}{2}(1 - x_{i'l})(1 - x_{j'l})\right] \quad (\text{A.8})$$

754 An estimate of the term  $\mathbb{E}_l[x_{il}x_{jl}]$  can be obtained by using the sample frequency of allele 1 in populations  
 755  $i$  and  $j$ . However, as we only have a sample from the population frequency we need to account for the finite  
 756 sampling bias within populations ( $i = j$ ). Let  $n$  be the sample size in population  $i$ , then

$$f_{ii} = \frac{\mathbb{E}_l[x_{ii}^2] \frac{n}{n-1} - \mathbb{E}_l[x_{ii}] \frac{1}{n-1} - \mathbb{E}_l[\epsilon_l^2]}{\mathbb{E}_l[\epsilon_l(1 - \epsilon_l)]} \quad (\text{A.9})$$

757 where our  $x$  are now sample frequencies. There is no finite-sample size correction for  $f_{ij}$ ,  $i \neq j$  and Equation  
 758 A.6 can be used directly.

759 In our simulations to show the effect of selection on the coancestry coefficients (Figure 3), we estimate  $f_{ij}$   
 760 in bins of fixed genetic size moving away from the selected site. We do this by approximating the expectations  
 761 in the numerator and denominators in Equations A.6 and A.9 by the average of the expression over all of  
 762 the SNPs that fall in a given genetic distance bin over all of the relevant simulations. To account for biases  
 763 induced by defining the allele of interest, we randomize the reference allele at each SNP.

## 764 A.2 Simulation implementation details

765 We perform coalescent simulations using `mssel`, a modified version of `ms` (Hudson, 2002) that allows  
766 for the incorporation of selection at single site (the code for this is provided in [https://github.com/  
767 kristinmlee/dmc](https://github.com/kristinmlee/dmc)). The program allows the user to specify the frequency trajectory of the selected allele  
768 through time across populations, this trajectory is then used to simulate genetic data under the coalescent  
769 model conditioning on this trajectory (using the sub-divided coalescent model Hudson and Kaplan (1988);  
770 Kaplan et al. (1991)). We generate stochastic trajectories for the selected allele across populations and  
771 describe the simulation process below. We simulate multiple instances of the stochastic trajectories and  
772 average our results across datasets generated for these trajectories. We focus on a set of four populations  
773 with relationships as shown in Figure 1. Populations 2 and 3 are adapted to a shared novel selection pressure  
774 and populations 1 and 4 are in the ancestral environment.

775 The original implementation of `mssel` assumes only a single origin of the selected allele, which occurs  
776 moving backward in time when the frequency of the derived allele goes to zero in the final population it  
777 segregates in. We modified the `mssel` source code directly to accommodate multiple origins of the selected  
778 allele as is necessary in the independent sweep model. We do so by allowing an independent origin of the  
779 selected allele in any population where the frequency of the derived selected allele goes to zero, if that  
780 population currently has a migration rate of zero to any other population containing the selected allele.

### 781 A.2.1 Generating stochastic trajectories for the selected allele

782 We generate stochastic trajectories for the selected allele to be used as input for `mssel` to generate sequence  
783 data for given convergent adaptation scenarios. We simulate the allele frequency trajectory for the selected  
784 allele forward in time using a normal deviate approximation to the simulation the Wright-Fisher diffusion.  
785 Specifically, given the frequency of the beneficial allele at time  $t$ ,  $X(t)$ , we simulate its frequency at time  
786  $t + \Delta t$  according to

$$X(t + \Delta t) \sim N(\mu_S(X(t))\Delta t, \sigma^2(X(t))\Delta t) \quad (\text{A.10})$$

787 where  $\mu_S(\cdot)$  and  $\sigma^2(\cdot)$  are the infinitesimal mean and variance of the Wright-Fisher diffusion. We set  
788  $\Delta t = 1/(2N)$ , representing one Wright-Fisher generation on the diffusion time-scale ( $2N$  generations). We  
789 set  $X(0) = g$ , the initial frequency of the beneficial allele. When selection starts from a new mutation,  
790  $g = 1/(2N)$ .

791 For all our models, the infinitesimal variance is

$$\sigma^2(X(t)) = X(t)(1 - X(t)), \quad (\text{A.11})$$

792 representing the effect of genetic drift.

793 For populations not impacted by migration, we condition our trajectory on the beneficial allele going to  
794 fixation forward in time. To do this we use the conditional infinitesimal mean

$$\mu_S(X(t)) = \frac{2NsX(t)(1 - X(t))}{\tanh(2NsX(t))} \quad (\text{A.12})$$

795 (see Przeworski et al., 2005; Berg and Coop, 2015, for previous applications). We simulate this process  
796 forward in time till fixation is reached.

797 **Migration model** In the case of our migration model, there is one way migration from population  $i$  into  $j$ .  
798 The trajectory of  $X_i$  is simulated first forwards in time, conditioning on fixation, using the above approach.  
799 We then simulate the frequency in population  $j$  starting from  $X_j(0) = 0$ , with the infinitesimal mean

$$\mu_S(X_j(t)) = 2NsX_j(t)(1 - X_j(t)) + 2Nm(X_i(t) - X_j(t)) \quad (\text{A.13})$$

800 (expanded from Ewens, 2004). We simulate the process forward in time until the selected allele reaches  
801 fixation in both populations. The first population to reach fixation is held at frequency 1 until the other  
802 population fixes for the beneficial allele.

803 **Standing variation model.** We define the standing variation trajectory as having three phases, the  
804 neutral phase, the standing phase, and the selected phase. To specify a trajectory in which the beneficial  
805 allele has been standing at frequency  $g$  for time  $t$ , we simply hold the allele frequency constant for this  
806 amount of time. We simulate a stochastic neutral trajectory of our beneficial allele from frequency  $g$  to 0  
807 backwards in time according to

$$X(t - \Delta t) \sim N(\mu_N(X(t))\Delta t, \sigma(X(t))\Delta t) \quad (\text{A.14})$$

808 using the infinitesimal mean conditional of the neutral allele going to loss

$$\mu_N(X(t)) = -X(t) \quad (\text{A.15})$$

809 (see Przeworski et al., 2005; Berg and Coop, 2015, for previous applications). We simulate the selection  
810 phase forward in time for  $2 \log(1/g)/s$  generations. If the beneficial allele has reached fixation before this  
811 time, it is held constant at frequency 1 for the remaining time. If not, the trajectory is simply stopped at  
812 this time. This allows for the interpretation of the standing time and the time of the onset of selection to  
813 be the same throughout simulations. For the whole trajectory of a beneficial allele, we paste together these  
814 three components: neutral increase of allele from frequency 0 to  $g$ , the standing phase at frequency  $g$  for  
815 time  $t$  generations, and the selective phase. For populations not experiencing selection, the beneficial allele  
816 is kept at frequency  $g$  for the entire length of the trajectory.

## 817 A.2.2 Details of coalescent simulations

818 In this section we give the details of the coalescent simulations, including the `mssel` command lines. The  
819 `mssel` input can be interpreted as follows,

```
820 ./mssel nsam_tot nreps nsam_anc nsam_der trajFile locSelSite -t  $\theta$  -r  $\rho$  nsites  
821 -I npops nAnc_pop1 nDerv_pop1 ... nAnc_popi nDerv_popi
```

822 For all of the simulations we generate neutral allele frequency data for 10 samples from each of 4 popula-  
823 tions. The populations are related to each other as shown in Figure 1. Note, we did 1000 replications of the  
824 simulations for parameters used to generate comparisons of average simulations coancestry coefficients com-  
825 pared to theoretical expectations. 100 replications were done for simulations used for parameter estimates  
826 and model comparisons. For simulations used for both, the first 100 runs were used.

827 **Independent sweep model.** We generated beneficial allele frequency trajectories under four different  
828 selection coefficients:  $s = [0.005, 0.01, 0.05, 0.1]$  under the independent sweep model with  $N_e = 100,000$ . We  
829 set  $r$ , the per generation probability of cross-over between ends of the simulated locus, to 0.005. The neutral  
830 mutation rate,  $\mu$ , for the entire locus is the same as  $r$ . `mssel` input for all independent sweep model is of the  
831 following form with different trajectory files for each  $s$ ,

```
./mssel 40 1000 20 20 ind_sel0.1_stochastic.traj 0 -t 2000 -r 2000 10000  
-I 4 10 0 0 10 0 10 10 0 -ej 0.05 3 4 -ej 0.05 2 1 -ej 0.07 4 1
```

832 We also simulate the same population structure with no selection to generate data to estimate the neutral  
833 coancestry matrix,  $\mathbf{F}$ , using `ms` as follows

```
834 ./ms 40 1000 -t 200 -r 2000 1000 -I 4 10 10 10 10 -ej 0.05 3 4 -ej 0.05 2 1 -ej 0.07 4 1
```

835 **Standing variation model.** With  $s = 0.01$  and  $g = 0.001$ , we generated beneficial allele frequency  
836 trajectories for standing times  $t = [50, 250, 500, 1000, 5000]$  generations under the standing variation model  
837 with  $N_e = 10,000$ . Our  $t$  references the time that the populations have been independent. Therefore,  
838 we adjusted the split times to ensure that the  $t$  of interest corresponded to the duration of time that the  
839 selected populations had the standing variant prior the populations joining in the ancestral population. The  
840 population split times were determined to ensure selection started after the populations were completely  
841 isolated and to maintain a similar ratio of time for 4 independent populations to 2 ancestral populations.  
842 We again set  $r = \mu = 0.005$ . The `ms` input was as follows,

```
./mssel 40 1000 20 20 sv_sel0.01_g0.001_t50_stochastic.traj 0 -t 200 -r 120 10000
-I 4 10 0 0 10 0 10 10 0 -ej 0.0346 2 1 -ej 0.0346 3 4 -ej 0.03575 4 1
./mssel 40 100 20 20 sv_sel0.01_g0.001_t250_stochastic.traj 0 -t 200 -r 200 10000
-I 4 10 0 0 10 0 10 10 0 -ej 0.039 3 4 -ej 0.039 2 1 -ej 0.0408 4 1
./mssel 40 1000 20 20 sv_sel0.01_g0.001_t500_stochastic.traj 0 -t 200 -r 200 10000
-I 4 10 0 0 10 0 10 10 0 -ej 0.04 2 1 -ej 0.04 3 4 -ej 0.047 4 1
./mssel 40 100 20 20 sv_sel0.01_g0.001_t1000_stochastic.traj 0 -t 200 -r 200 10000
-I 4 10 0 0 10 0 10 10 0 -ej 0.04 3 4 -ej 0.04 2 1 -ej 0.0595 4 1
./mssel 40 1000 20 20 sv_sel0.01_g0.001_t5000_stochastic.traj 0 -t 200 -r 200 10000
-I 4 10 0 0 10 0 10 10 0 -ej 0.135 2 1 -ej 0.135 3 4 -ej 0.1595 4 1
```

843 We also simulated under two additional selection coefficients,  $s = [0.001, 0.05]$ , keeping  $t = 500$  and  
844  $g = 0.001$ .

```
./mssel 40 100 20 20 sv_sel0.001_g0.001_t500_stochastic.traj 0 -t 200 -r 200 10000
-I 4 10 0 0 10 0 10 10 0 -ej 0.3455 3 4 -ej 0.3455 2 1 -ej 0.3578 4 1
./mssel 40 100 20 20 sv_sel0.05_g0.001_t500_Ne10000_stochastic.traj 0 -t 200 -r 200 10000
-I 4 10 0 0 10 0 10 10 0 -ej 0.00695 3 4 -ej 0.00695 2 1 -ej 0.01935 4 1
```

845 Again, neutral regions were simulated in ms using the same population structure (i.e. each parameter  
846 set had its own neutral data generated).

847 **Migration model.** Lastly, we simulated under the migration model with  $m = [0.0001, 0.001, 0.01, 0.1]$ ,  
848 holding  $s = 0.01$  for  $N_e = 10,000$ . Again, we simulated 10 samples from 4 populations related to each other  
849 as specified in Figure 1. Now, in mssel, we specify migration to start just prior to origin of the beneficial allele  
850 in the source population. We set population 2 to be the source and have  $4N_e m$  migrants from population 2  
851 into population 3 each generation. We again set  $r = \mu = 0.005$ . Thus,

```
./mssel 40 1000 20 20 mig_sel0.01_migle-04_stochastic.traj 0 -t 200 -r 200 10000
-I 4 10 0 0 10 0 10 10 0 -ej 0.07 2 1 -ej 0.07 3 4 -ej 0.1 4 1
-em 0.059 3 2 0 -em 0 3 2 4
./mssel 40 1000 20 20 mig_sel0.01_mig0.001_stochastic.traj 0 -t 200 -r 200 10000
-I 4 10 0 0 10 0 10 10 0 -ej 0.07 2 1 -ej 0.07 3 4 -ej 0.1 4 1
-em 0.059 3 2 0 -em 0 3 2 40
./mssel 40 1000 20 20 mig_sel0.01_mig0.01_stochastic.traj 0 -t 200 -r 200 10000
-I 4 10 0 0 10 0 10 10 0 -ej 0.07 2 1 -ej 0.07 3 4 -ej 0.1 4 1
-em 0.059 3 2 0 -em 0 3 2 400
./mssel 40 1000 20 20 mig_sel0.01_mig0.1_stochastic.traj 0 -t 200 -r 200 10000
-I 4 10 0 0 10 0 10 10 0 -ej 0.07 2 1 -ej 0.07 3 4 -ej 0.1 4 1
-em 0.059 3 2 0 -em 0 3 2 4000
```

852 We also simulated under two additional selection coefficients,  $s = [0.005, 0.05]$ , keeping  $m = 0.001$ .

```
./mssel 40 100 20 20 mig_sel0.05_mig0.001_stochastic.traj 0 -t 200 -r 200 10000
-I 4 10 0 0 10 0 10 10 0 -ej 0.021 2 1 -ej 0.021 3 4 -ej 0.03 4 1
-em 0.014 3 2 0 -em 0 3 2 40
./mssel 40 100 20 20 mig_sel0.005_mig0.001_stochastic.traj 0 -t 200 -r 200 10000
-I 4 10 0 0 10 0 10 10 0 -ej 0.12 2 1 -ej 0.12 3 4 -ej 0.17 4 1
-em 0.11 3 2 0 -em 0 3 2 40
```

853 Neutral regions were again simulated using ms. Each set of parameters has its own neutral data generated  
854 as the migration rate impacts neutral coancestry as well.

### 855 A.2.3 Interpreting mssel output

856 The output from mssel and ms is in the form of haplotypes for each of the sampled chromosomes at polymor-  
857 phic sites in addition to their positions on a scale of (0, 1). We use this to calculate sample allele frequencies

858 at each site for each population. Prior to performing further estimations or analyses with these neutral allele  
859 frequencies, we randomize the reference allele so that there is no bias resulting from which allele was called  
860 ancestral or derived. We exclude sites where the average allele frequencies across populations are less than  
861 5% or greater than 95%.

#### 862 **A.2.4 Composite likelihoods of simulated data under all models details**

863 We calculated the composite log-likelihoods of each the simulated datasets under all models, including the  
864 neutral model, with the same parameter space shown in Table S1.

#### 865 **A.2.5 Maximum likelihood estimate of parameters from simulated data under correct model**

866 We also calculated the composite log-likelihoods of each the simulated datasets under the correct model used  
867 to generate the data now with a more dense grid of parameters to obtain better estimates of the MCLE of  
868 each parameter. We allowed  $g$  to vary in the calculations of the MCLEs under the standing variation model.  
869 See Table S2, Table S4, Table S5.

#### 870 **A.2.6 Inference details: mean-centering allele frequencies and covariances, sample size cor- 871 rection, and speed-ups**

872 Given that we do not know the true ancestral mean at locus  $l$ ,  $\epsilon_l$ , we use the mean of the present-day sample  
873 allele frequencies at this locus,  $\bar{x}_l = \frac{1}{k} \sum_{i=1}^K x_{i,l}$ . When mean-centering, we lose a degree of freedom so in  
874 calculating the likelihood it is necessary to drop information from one population. Since the information  
875 from the dropped population is incorporated in the mean, the choice of the dropped population is arbitrary.  
876 In matrix form, the mean-centered allele frequencies with one dropped population can be expressed as

$$\vec{x}'_i = \mathbf{T}\vec{x}_i \quad (\text{A.16})$$

877 where  $\mathbf{T}$  is an  $K - 1$  by  $K$  matrix with  $\frac{K-1}{K}$  on the main diagonal and  $-\frac{1}{K}$  elsewhere. Prior to mean-  
878 centering, we randomize the reference allele at each SNP to account for biases induced by defining the allele  
879 of interest.

880 Now, we model the mean-centered allele frequencies as multivariate normal around mean zero with  
881 covariance proportional to a mean-centered parameterized covariance matrix ( $\mathbf{F}^{(S)'}$ ) as

$$\vec{x}'_i \sim \mathcal{N}\left(\vec{0}, \bar{x}_l(1 - \bar{x}_l)\mathbf{F}^{(S)'}\right) \quad (\text{A.17})$$

882 where we use the average present day allele frequency across populations at the locus,  $\bar{x}_l$ , as an estimate of  $\epsilon_l$   
883 in the site-specific term in the covariance. We note that  $\bar{x}_l(1 - \bar{x}_l)$  is a slightly downwardly biased estimate  
884 of  $\epsilon(1 - \epsilon)$ , but for our purposes it seems sufficient to include this term as a locus-specific adjustment to the  
885 expected covariance.

886 To obtain the corresponding mean-centered covariance matrix, dropping the same population, we can  
887 apply the following matrix operations,

$$\mathbf{F}^{(S)'} = \mathbf{T}\mathbf{F}^{(S)}\mathbf{T}^\top. \quad (\text{A.18})$$

888 this new matrix is  $K - 1$  by  $K - 1$  and full rank.

889 Before mean-centering,  $\mathbf{F}^{(S)}$ , we apply a sample size correction to correct for the finite sampling bias.  
890 We add  $1/n_i$  to the diagonal where  $n_i$  is the sample size in population  $i$ . We take twice the number of  
891 diploid individuals sampled in population  $i$  as  $n_i$  for data applications. In simulations, we use the number of  
892 chromosomes sampled in population  $i$  as  $n_i$ . Note that both this mean-centering and sample size correction  
893 is also preformed on the neutral matrix,  $\mathbf{F}$  before likelihood calculations under a neutral model with no  
894 selection.

895 To decrease some of the computational time involved in our likelihood calculations, we precompute the  
896 mean-centered covariance matrices with selection,  $\mathbf{F}^{(S)'}$ , for given bins of distance away from a putative  
897 selected site. We first divide our distances in our window into 1000 bins and take the midpoint of the  
898 distances in these bins to calculate  $\mathbf{F}^{(S)'}$  as this matrix is a function of distance. To avoid the costly step  
899 of recomputing the corresponding inverses and determinants needed for likelihood calculations, we do this

900 step first and use these values for all SNPs in a given bin, and store them and reuse them over all locations  
 901 of the selected site.

902 Thus, we calculate the likelihood of mean-centered allele frequencies,  $\vec{x}_l'$ , given our model  $M$  and its  
 903 parameters  $\Theta_M$ , a given locus  $l$  as

$$P(\vec{x}_l' | \mathbf{F}^{(S)'}) (r_l, M, \Theta_M) = \frac{\exp(-\frac{1}{2} \vec{x}_l'^{\top} (\mathbf{F}^{(S)'})^{-1} (\vec{x}_l(1 - \vec{x}_l))^{-1} \vec{x}_l')}{\sqrt{2\pi^k (\vec{x}_l(1 - \vec{x}_l))^k \det \mathbf{F}^{(S)'}}} \quad (\text{A.19})$$

904 where  $k = K - 1$ , the rank of matrix  $\mathbf{F}^{(S)'}$ .

### 905 A.3 Standing variant model with a source population

906 When there are multiple selected populations and they do not follow a bifurcating tree structure, it is  
 907 necessary to incorporate a model that has a source population for the standing variant to have self-consistent  
 908 mean-centered covariance matrices.

909 Let population  $l$  be a selected population and the source of the beneficial allele. In all other populations,  
 910 the beneficial allele is standing for time  $t$  generations at frequency  $g$  before the lineage returns to the  
 911 source population where it still standing at frequency  $g$  (see Figure 11). We can define pairwise coancestry  
 912 coefficients for all pairs of populations under this model. Let populations  $i$  and  $j$  represent populations that  
 913 experience selection and population  $k$  be any unselected population.

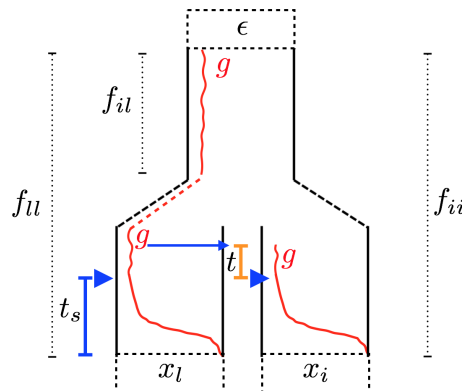


Figure 11: Trajectories of the beneficial allele (red) for the standing variant model with a source population. Populations  $l$  and  $i$  are under selection with present-day allele frequencies  $x_l$  and  $x_i$  at a neutral locus, derived from an ancestral population with allele frequency  $\epsilon$ . The populations share some amount of drift proportional to  $f_{il}$  before reaching the ancestral population. The beneficial allele is standing at frequency  $g$  in the source population,  $l$ . It migrates into population  $i$  from  $l$ , where it is standing at frequency  $g$  for  $t$  generations prior to the onset of selection, indicated by the blue triangles.

914 Since population  $l$  is the source, its variance follows the same form as Equation 7.

$$f_{il}^{(S)} = y^2 \left( \frac{1}{1 + 4N_e r g} + \frac{4N_e r g}{1 + 4N_e r g} f_{il} \right) + (1 - y^2) f_{il} \quad (\text{A.20})$$

915 All other selected populations have a modified variance since lineages that fail to recombine off the  
 916 beneficial background during the sweep and fail to coalesce or recombine during the standing phase return

917 to the source population. Thus,

$$\begin{aligned}
 f_{ii}^{(S)} &= (1-y)^2 f_{ii} + 2y(1-y)(r_t f_{il} + (1-r_t) f_{ii}) + y^2 \left( e^{-t(2r + \frac{1}{2N_e g})} \left( \frac{1}{1+4N_e r g} + \frac{4N_e r g}{1+4N_e r g} f_{il} \right) \right. \\
 &\quad + (1 - e^{-t(2r + \frac{1}{2N_e g})}) \frac{1}{1+4N_e r g} + \left( (1 - e^{-t(2r + \frac{1}{2N_e g})}) \frac{4N_e r g}{1+4N_e r g} - (1 - e^{-t(r + \frac{1}{2N_e g})}) \frac{4N_e r g}{1+2N_e r g} r_t \right) f_{ii} \\
 &\quad \left. + (1 - e^{-t(r + \frac{1}{2N_e g})}) \frac{4N_e r g}{1+2N_e r g} r_t f_{il} \right)
 \end{aligned}
 \tag{A.21}$$

918 There is additional coancestry between pairs of selected populations. This takes a different form than  
 919 Equation 9 as there since if either lineage fails to recombines off the beneficial background during the sweep  
 920 or standing phase, the lineage will be in population  $l$ . For selected populations  $i$  and  $j$ , now

$$\begin{aligned}
 f_{ij}^{(S)} &= (1-y)^2 f_{ij} + y^2 \left( r_t^2 \left( \frac{1}{1+4N_e r g} + \frac{4N_e r g}{1+4N_e r g} f_{il} \right) + (1-r_t)^2 f_{ij} + r_t(1-r_t)(f_{il} + f_{jl}) \right) \\
 &\quad + y(1-y) \left( 2(1-r_t) f_{ij} + r_t(f_{il} + f_{jl}) \right)
 \end{aligned}
 \tag{A.22}$$

921 If either population is the source,  $l$  this reduces to

$$f_{il}^{(S)} = y r_t \left( y r_t \left( \frac{1}{1+4N_e r g} + \frac{4N_e r g}{1+4N_e r g} f_{il} \right) + (1-y r_t) f_{il} \right) + (1-y r_t) f_{il}
 \tag{A.23}$$

922 since if the lineage fails to recombines off the beneficial background in population  $i$ , it is back in population  $l$ .  
 923 If the lineage in  $l$  is still on the beneficial background after the sweep and the initial  $t$  generations of standing,  
 924 they can coalesce during the standing phase in population  $l$ . Else, the lineages will coalesce neutrally in  
 925 population  $l$ . However, if the lineage sampled in population  $i$  does not return to the source population (i.e.  
 926 it recombines during the sweep or standing phase of  $t$  generations), the lineages can coalesce with neutral  
 927 probability  $f_{il}$ .

928 Lastly, we must incorporate the impact linked selection has on the coancestry between lineages sampled  
 929 from any pair of non-source selected population  $i$  and non-selected population  $k$ .

$$f_{ik}^{(S)} = y \left( r_t f_{kl} + (1-r_t) f_{ik} \right) + (1-y) f_{ik}
 \tag{A.24}$$

930 Since lineages that do not recombine off the beneficial background in population  $i$  go back into the source  
 931 population  $l$ , non-selected populations may now have more or less coancestry with population  $i$  depending  
 932 on whether  $l$  is neutrally has more or less coancestry with population  $l$ , respectively.

## 934 A.4 Migration model extensions

### 935 A.4.1 Single pulses of migration

936 We also considered models of a single pulse of migration. We solve for  $f_{ii}^{(S)}$  and  $f_{ij}^{(S)}$  for the bounds on  
 937 the time during which the beneficial allele could migrate: (1) “instantly” after the beneficial allele arises in  
 938 population  $i$  and (2) after the beneficial allele reaches fixation in the population  $i$ .

939 **Beneficial allele migrates instantly after it arises in population  $i$ .** In this case, we are specifying  
 940 the pulse of migration from population  $i$  into population  $j$  occurs sufficiently soon enough after the sweep  
 941 began such that the entire haplotype the beneficial mutation arises on in population  $i$  migrates to population  
 942  $j$  (i.e. there is no time for recombination to occur). This case gives us results for an extreme of a single  
 943 pulse of migration may not be particularly relevant as the spread of the beneficial allele into population  $j$   
 944 will likely only occur after it has reached a sufficiently high frequency in population  $i$  as it may be lost due  
 945 to drift. However, these results aid in our intuition of this model.



946 As the beneficial allele originates in population  $i$ , again,

$$f_{ii}^{(S)} = (f_{ii} + y^2(1 - f_{ii})). \quad (\text{A.25})$$

947 The probability of two lineages in the recipient population,  $j$ , coalescing before reaching the ancestral  
948 population is now

$$f_{jj}^{(S)} = y^2 + 2y(1 - y)f_{ij} + (1 - y)^2 f_{jj} \quad (\text{A.26})$$

949 Here, both lineages can not recombine off the sweep (w.p.  $y^2$ ) and therefore coalesce with probability 1.  
950 Exactly one lineage can recombine off the sweep (w.p.  $2y(1 - y)$ ) and therefore the two lineages can only  
951 coalesce in the shared drift phase (w.p.  $f_{ij}$ ) as the lineage that does not recombine off the sweep migrates  
952 into population  $i$ . Both lineages can recombine off the sweep (w.p.  $(1 - y)^2$ ) and then can coalesce in  
953 population  $j$  before they reach the ancestral population.

954 The probability of two lineages drawn from each population coalescing before reaching the ancestral  
955 population is

$$f_{ij}^{(S)} = (1 - y)f_{ij} + y(y + (1 - y)f_{ii}) \quad (\text{A.27})$$

957 In this case, if the lineage in population  $j$  recombines off the sweep (w.p.  $1 - y$ ), the two lineages can  
958 only coalesce in the shared drift phase (w.p.  $f_{ij}$ ) before reaching the ancestral population. If the lineage in  
959 population  $j$  fails to recombine off the sweep (w.p.  $y$ ), it migrates back to population  $i$  and will be forced  
960 to coalesce with the lineage in population  $i$  if it also failed to recombine, else they will coalesce neutrally in  
961 population  $i$ .

962 **Beneficial allele migrates after it reaches fixation in population  $i$ .** For the coancestry coefficient  
963 for population  $j$ , the logic follows from that of when the pulse of migration happens instantly. However  
964 in deriving the coancestry coefficient between populations  $i$  and  $j$ , in the case where the lineage sampled  
965 from population  $j$  fails to recombine off the sweep and migrates back to population  $i$ , which happens with  
966 probability  $y$ , it is like we have two lineages sampled in population  $i$ . Now, both could either fail to  
967 recombine off the sweep and coalesce with probability 1 or one or both could recombine off the sweep and  
968 coalesce neutrally in population  $i$ . This can be written as

$$f_{ij}^{(S)} = (1 - y)f_{ij} + y(y^2 + (1 - y^2)f_{ii}) \quad (\text{A.28})$$

969 Together, these results characterize the other end point of a single pulse of migration spreading the  
970 beneficial allele to the recipient population.

## 971 A.5 Forward in time derivation examples

972 For the forward in time results we utilize Gillespie's (2000) pseudohitchhiking approximation with the incor-  
973 poration of recombination to model the variance in the change in neutral allele frequencies due to a selective  
974 sweep ( $\Delta_S x_i$  for population  $i$ ). A new beneficial mutation will arise on the same background as a neutral  
975 allele with probability equal to its frequency in the population,  $x$ . In the case no crossing over occurs and  
976 the new mutation sweeps to fixation, the neutral allele frequency after the hitchhiking event,  $x'$ , will either  
977 be 1 with probability  $x$  or 0 with probability  $1 - x$ . Therefore,

$$\Delta_S x = \begin{cases} (1 - x) & \text{with probability } x \\ -x & \text{with probability } (1 - x) \end{cases} \quad (\text{A.29})$$

978 thus  $\mathbb{E}[\Delta_S x] = 0$  and  $\text{Var}[\Delta_S x] = x(1 - x)$ .

979 Recombination can be incorporated into this model, allowing the neutral allele stop hitchhiking before  
980 it reaches fixation. The frequency of the haplotype on which the favorable mutation arises will increase to  
981  $y$  and all other alleles will have their frequencies reduced by  $1 - y$ . So, if the favorable allele appears on  
982

983 the same background of our neutral allele, which happens with probability  $x$ ,  $x' = (1 - y)x + y$ . Else, with  
 984 probability  $1 - x$ ,  $x' = (1 - y)x$ . Therefore,

$$\Delta_S x = \begin{cases} y(1 - x) & \text{with probability } x \\ -yx & \text{with probability } (1 - x) \end{cases} \quad (\text{A.30})$$

985 thus with recombination,  $\mathbb{E}[\Delta_S x] = 0$  and  $\text{Var}[\Delta_S x] = y^2 x(1 - x)$ .

986 We can break down the changes in allele frequencies in the two populations from the ancestral allele  
 987 frequency  $\epsilon$  into three components if we assume the independent drift in each population after the sweep  
 988 is negligible: the change due to (1) shared drift between populations  $i$  and  $j$  before they split ( $\Delta_N x_{ij}$ ),  
 989 (2) independent drift in each population before the sweep ( $\Delta_N x_i$  and  $\Delta_N x_j$ ), and (3) the selective sweep  
 990 occurring in each population ( $\Delta_S x_i$  and  $\Delta_S x_j$ ).

991 Define  $\mathbb{E}[\Delta_N x_{ij}^2] = \epsilon(1 - \epsilon)f_{ij}$  and  $\mathbb{E}[\Delta_N x_i^2] = \epsilon(1 - \epsilon)f_i$  for population  $i$ . The total amount of vari-  
 992 ance in a neutral allele frequency for the  $i$ th population is defined as  $\epsilon(1 - \epsilon)f_{ii}$  which we approximate as  
 993  $\epsilon(1 - \epsilon)(f_{ij} + f_i)$ . This only holds if we assume the time intervals are short relative to drift so that these  
 994 terms act additively. If this is not the case, the  $\mathbb{E}[\Delta_N x_i^2]$  is no longer the probability that two alleles drawn  
 995 from population  $i$  before the sweep begins are identical by descent with reference to the ancestral population  
 996 with neutral allele frequency  $\epsilon$ , but rather with reference to the population before the split into populations  
 997  $i$  and  $j$  with neutral allele frequency  $x_{ij}$ . A more careful treatment of these parameters could be done to  
 998 relax this assumption, and follows naturally in a coalescent setting.

1000

1001 From a forward in time perspective, we can solve for  $\text{Var}[\Delta x_i]$ ,  $\text{Var}[\Delta x_j]$ , and  $\text{Cov}[\Delta x_i, \Delta x_j]$  with  $\Delta x_i =$   
 1002  $\Delta_N x_{ij} + \Delta_N x_i + \Delta_S x_i$ . Assuming drift terms are independent of each other, we are left with the following  
 1003 expressions

$$\text{Var}[\Delta x_i] = \epsilon(1 - \epsilon)f_{ii} + \mathbb{E}[\Delta_S x_i^2] + 2\mathbb{E}[\Delta_N x_{ij} \cdot \Delta_S x_i] + 2\mathbb{E}[\Delta_N x_i \cdot \Delta_S x_i] \quad (\text{A.31})$$

1004 and

$$\text{Cov}[\Delta x_i, \Delta x_j] = \epsilon(1 - \epsilon)f_{ij} + \mathbb{E}[\Delta_N x_{ij} \cdot \Delta_S x_i] + \mathbb{E}[\Delta_N x_{ij} \cdot \Delta_S x_j] + \mathbb{E}[\Delta_N x_i \cdot \Delta_S x_j] + \mathbb{E}[\Delta_S x_i \cdot \Delta_S x_j] \quad (\text{A.32})$$

### 1005 A.5.1 Independent sweep model

In the case of independent sweeps where there is no gene flow between populations, many terms in Equations  
 A.31 and A.32 equal zero since the sweeps are independent. For the variances, we are left with

$$\begin{aligned} \text{Var}[\Delta x_i] &= \epsilon(1 - \epsilon)f_{ii} + \mathbb{E}[\Delta_S x_i^2] \\ &= \epsilon(1 - \epsilon)(f_{ii} + y^2(1 - f_{ii})) \end{aligned} \quad (\text{A.33})$$

1006 The covariance in allele frequencies between populations  $i$  and  $j$ , is simply what we would expect under  
 1007 neutrality.

$$\text{Cov}[\Delta x_1, \Delta x_2] = \epsilon(1 - \epsilon)f_{ij} \quad (\text{A.34})$$

### 1008 A.5.2 Shared sweeps via migration

1009 The migration models better exemplifies these forward in time calculations. We demonstrate the calculations  
 1010 of  $\text{Var}[\Delta x_j]$  and  $\text{Cov}[\Delta x_i, \Delta x_j]$  for pulse of migration models specified in A.4.

1011 **Beneficial allele migrates instantly after it arises in population  $i$ .** The background on which  
 1012 the beneficial mutation arises depends on the neutral allele frequency in population  $i$  before the sweep,  $x_i$ .  
 1013 We are specifying the pulse of migration from population  $i$  into population  $j$  occurs sufficiently soon enough  
 1014 after the sweep began such that the entire haplotype the beneficial mutation arises on in population  $i$  mi-  
 1015 grates to population  $j$  (i.e. there is no time for recombination to occur). Now  $\Delta_S x_j$  depends on the neutral

1016 allele frequency in population  $i$  before the sweep.

1017

$$\Delta_S x_j = \begin{cases} y(1 - (\epsilon + \Delta_N x_{ij} + \Delta_N x_j)) & \text{with probability } \epsilon + \Delta_N x_{ij} + \Delta_N x_i \\ -y(\epsilon + \Delta_N x_{ij} + \Delta_N x_j) & \text{with probability } (1 - (\epsilon + \Delta_N x_{ij} + \Delta_N x_i)) \end{cases} \quad (\text{A.35})$$

1018

1019

1020 As the beneficial allele originates in population  $i$ , again,

$$\text{Var}[\Delta x_i] = \epsilon(1 - \epsilon)(f_{ii} + y^2(1 - f_{ii})). \quad (\text{A.36})$$

1021

1022

Now  $\Delta_S x_j$  depends on  $x_i$ ,  $\mathbb{E}[\Delta_N x_i \cdot \Delta_S x_j]$ ,  $\mathbb{E}[\Delta_S x_i \cdot \Delta_S x_j]$ , and  $\mathbb{E}[\Delta_N x_{ij} \cdot \Delta_S x_j]$  are no longer zero. So,

$$\begin{aligned} \text{Var}[\Delta x_j] &= \epsilon(1 - \epsilon)f_{jj} + 2\mathbb{E}[\Delta_N x_{ij} \cdot \Delta_S x_j] + \mathbb{E}[\Delta_S x_j^2] \\ &= \epsilon(1 - \epsilon)(f_{jj} - 2yf_j + y^2(1 + f_j - f_{ij})) \end{aligned} \quad (\text{A.37})$$

and

$$\begin{aligned} \text{Cov}[\Delta x_i, \Delta x_j] &= \epsilon(1 - \epsilon)f_{ij} + \mathbb{E}[\Delta_N x_i \cdot \Delta_S x_i] + \mathbb{E}[\Delta_S x_i \cdot \Delta_S x_j] \\ &= \epsilon(1 - \epsilon)(f_{ij} + yf_i + y^2(1 - f_i - f_{ij})). \end{aligned} \quad (\text{A.38})$$

1023

1024

This result is the same as Equation A.27 if the assumption about drift being additive holds such that  $f_{ii} = f_i + f_{ij}$ .

1025

1026

**Beneficial allele migrates after it reaches fixation in population  $i$ .** Now, the frequency of a neutral allele in population  $i$  after the sweep has occurred is

$$x_{i'} = \begin{cases} y + (1 - y)x_i & \text{with probability } x_i \\ (1 - y)x_i & \text{with probability } (1 - x_i) \end{cases}$$

1027

Fixing that the migration from population  $i$  into  $j$  occurs after the sweep has finished in population  $i$ ,

$$\Delta_S x_j = \begin{cases} y(1 - (\epsilon + \Delta_N x_{ij} + \Delta_N x_j)) & \text{with probability } \epsilon + \Delta_N x_{ij} + \Delta_N x_i + \Delta_S x_i \\ -y(\epsilon + \Delta_N x_{ij} + \Delta_N x_j) & \text{with probability } (1 - (\epsilon + \Delta_N x_{ij} + \Delta_N x_i - \Delta_S x_i)) \end{cases} \quad (\text{A.39})$$

1028

This can also be written as

$$\Delta_S x_j = \begin{cases} y(1 - x_j) & \text{with probability } x_i(y + (1 - y)x_i) \\ y(1 - x_j) & \text{with probability } (1 - x_i)(1 - y)x_i \\ -yx_j & \text{with probability } x_i(1 - y - (1 - y)x_i) \\ -yx_j & \text{with probability } (1 - x_i)(1 - (1 - y)x_i) \end{cases} \quad (\text{A.40})$$

1029

1030

1031

1032

1033

1034

1035

1036

Here, the first case is that the beneficial allele arises on the same background as our neutral allele in population  $i$  and then is the haplotype that migrates into population  $j$ . The probability of the haplotype migrating is equal to its frequency in the population. The third case also includes the beneficial allele arising on the same background as our neutral allele, but the other haplotype migrates. The second and fourth cases are when the beneficial mutation arises on the other background as our neutral allele. In the second case, the haplotype containing our neutral allele migrates after the sweep and in the fourth, the other haplotype migrates.

1037

1038

1039

The variance within population  $i$  and population  $j$  are the same as in the case of the beneficial allele migrating instantly. The only term changed by specifying that the pulse of migration happens after the sweep is  $\mathbb{E}[\Delta_S x_i \cdot \Delta_S x_j]$  which is now  $\epsilon(1 - \epsilon)y^3(1 - f_{jj})$ . So,

$$\text{Cov}[\Delta x_i, \Delta x_j] = \epsilon(1 - \epsilon)(f_{ij} + yf_j + y^3(1 - f_j - f_{ij})) \quad (\text{A.41})$$

## References

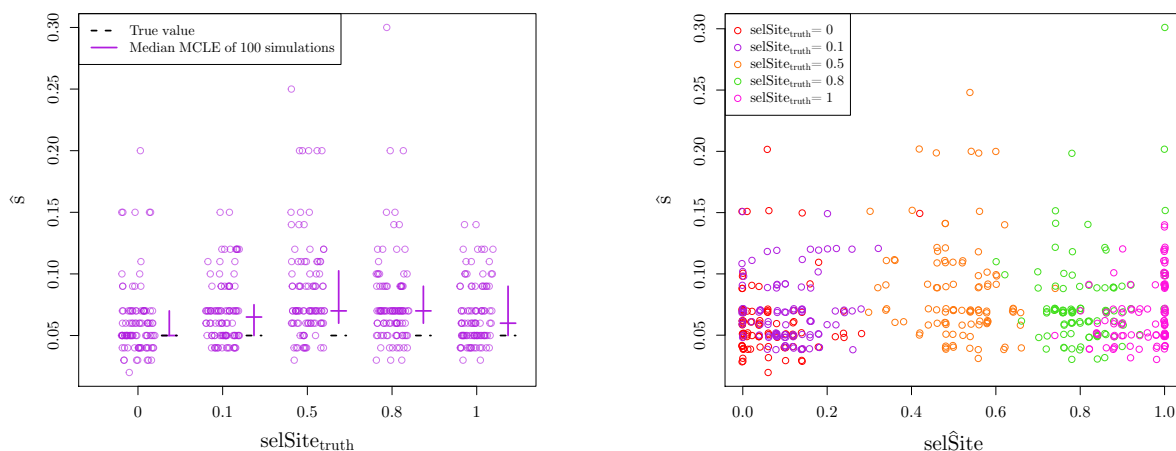
- 1041 Arendt, J. and D. Reznick (2008). Convergence and parallelism reconsidered: what have we learned about  
1042 the genetics of adaptation? *Trends in Ecology and Evolution* 23(1), 26 – 32.
- 1043 Barrett, R. D. and D. Schluter (2008). Adaptation from standing genetic variation. *Trends in ecology &*  
1044 *evolution* 23(1), 38–44.
- 1045 Barton, N. (1998). The effect of hitch-hiking on neutral genealogies. *Genet. Res.* 72, 123–133.
- 1046 Barton, N. and B. O. Bengtsson (1986, Dec). The barrier to genetic exchange between hybridising popula-  
1047 tions. *Heredity* 57(3), 357–376.
- 1048 Berg, J. J. and G. Coop (2015). A coalescent model for a sweep of a unique standing variant. *Genetics* 201(2),  
1049 707–725.
- 1050 Bierne, N. (2010). The distinctive footprints of local hitchhiking in a varied environment and global hitch-  
1051 hiking in a subdivided population. *Evolution* 64(11), 3254–3272.
- 1052 Chan, Y. F., M. E. Marks, F. C. Jones, G. Villarreal, M. D. Shapiro, S. D. Brady, A. M. Southwick, D. M.  
1053 Absher, J. Grimwood, J. Schmutz, et al. (2010). Adaptive evolution of pelvic reduction in sticklebacks by  
1054 recurrent deletion of a *pitx1* enhancer. *science* 327(5963), 302–305.
- 1055 Charlesworth, B., M. Nordborg, and D. Charlesworth (1997, Oct). The effects of local selection, balanced  
1056 polymorphism and background selection on equilibrium patterns of genetic diversity in subdivided popu-  
1057 lations. *GenetRes* 70(2), 155–174.
- 1058 Chen, H., N. Patterson, and D. Reich (2010). Population differentiation as a test for selective sweeps.  
1059 *Genome research* 20(3), 393–402.
- 1060 Colosimo, P. F., K. E. Hosemann, S. Balabhadra, G. Villarreal, M. Dickson, J. Grimwood, J. Schmutz, R. M.  
1061 Myers, D. Schluter, and D. M. Kingsley (2005). Widespread parallel evolution in sticklebacks by repeated  
1062 fixation of ectodysplasin alleles. *science* 307(5717), 1928–1933.
- 1063 Coop, G., D. Witonsky, A. Di Rienzo, and J. K. Pritchard (2010). Using environmental correlations to  
1064 identify loci underlying local adaptation. *Genetics* 185(4), 1411–1423.
- 1065 DeGiorgio, M., K. E. Lohmueller, and R. Nielsen (2014). A model-based approach for identifying signatures  
1066 of ancient balancing selection in genetic data. *PLoS Genet* 10(8), e1004561.
- 1067 Duvernell, D. D., J. B. Lindmeier, K. E. Faust, and A. Whitehead (2008). Relative influences of historical  
1068 and contemporary forces shaping the distribution of genetic variation in the atlantic killifish, *fundulus*  
1069 *heteroclitus*. *Molecular Ecology* 17(5), 1344–1360.
- 1070 Ewens, W. (2004). *Mathematical Population Genetics 1: Theoretical Introduction*. Interdisciplinary Applied  
1071 Mathematics. Springer New York.
- 1072 Gillespie, J. H. (2000). Genetic drift in an infinite population. The pseudohitchhiking model. *Genetics* 155,  
1073 909–919.
- 1074 Guerrero, R. F., F. Rousset, and M. Kirkpatrick (2012). Coalescent patterns for chromosomal inversions in  
1075 divergent populations. *Phil. Trans. R. Soc. B* 367(1587), 430–438.
- 1076 Harvey, P. H. and M. D. Pagel (1991). *The comparative method in evolutionary biology*, Volume 239. Oxford  
1077 university press Oxford.
- 1078 Hedrick, P. W. (2013). Adaptive introgression in animals: examples and comparison to new mutation and  
1079 standing variation as sources of adaptive variation. *Molecular ecology* 22(18), 4606–4618.
- 1080 Heliconius Genome Consortium (2012). Butterfly genome reveals promiscuous exchange of mimicry adapta-  
1081 tions among species. *Nature* 487(7405), 94–98.

- 1082 Hudson, R. R. (2001). Two-locus sampling distributions and their application. *Genetics* 159(4), 1805–1817.
- 1083 Hudson, R. R. (2002). Generating samples under a Wright–Fisher neutral model of genetic variation.  
1084 *Bioinformatics* 18, 337–338.
- 1085 Hudson, R. R. and N. L. Kaplan (1988). The coalescent process in models with selection and recombination.  
1086 *Genetics* 120(3), 831–840.
- 1087 Jones, F. C., M. G. Grabherr, Y. F. Chan, P. Russell, E. Mauceli, J. Johnson, R. Swofford, M. Pirun,  
1088 M. C. Zody, S. White, E. Birney, S. Searle, J. Schmutz, J. Grimwood, M. C. Dickson, R. M. Myers, C. T.  
1089 Miller, B. R. Summers, A. K. Knecht, S. D. Brady, H. Zhang, A. A. Pollen, T. Howes, C. Amemiya,  
1090 J. Baldwin, T. Bloom, D. B. Jaffe, R. Nicol, J. Wilkinson, E. S. Lander, F. Di Palma, K. Lindblad-Toh,  
1091 and D. M. Kingsley (2012, Apr). The genomic basis of adaptive evolution in threespine sticklebacks.  
1092 *Nature* 484(7392), 55–61.
- 1093 Kaplan, N., R. R. Hudson, and M. Iizuka (1991). The coalescent process in models with selection, recombina-  
1094 tion and geographic subdivision. *Genetical research* 57(01), 83–91.
- 1095 Kaplan, N. L., R. R. Hudson, and C. H. Langley (1989, December). The “hitchhiking effect” revisited.  
1096 *Genetics* 123, 887–899.
- 1097 Kelly, J. K. and M. J. Wade (2000). Molecular evolution near a two-locus balanced polymorphism. *Journal*  
1098 *of Theoretical Biology* 204(1), 83 – 101.
- 1099 Kim, Y. and T. Maruki (2011). Hitchhiking effect of a beneficial mutation spreading in a subdivided  
1100 population. *Genetics* 189(1), 213–226.
- 1101 Kim, Y. and R. Nielsen (2004). Linkage disequilibrium as a signature of selective sweeps. *Genetics* 167(3),  
1102 1513–1524.
- 1103 Kim, Y. and W. Stephan (2002). Detecting a local signature of genetic hitchhiking along a recombining  
1104 chromosome. *Genetics* 160, 765–777.
- 1105 Kirkpatrick, M. (2010). How and why chromosome inversions evolve. *PLoS Biol* 8(9), e1000501.
- 1106 Larribe, F. and P. Fearnhead (2011). On composite likelihoods in statistical genetics. *Statistica Sinica*,  
1107 43–69.
- 1108 Lee, Y. W. (2009). *Genetics Analysis of Standing Variation for Floral Morphology and Fitness Components*.  
1109 Ph. D. thesis, Duke University.
- 1110 Lipson, M., P.-R. Loh, A. Levin, D. Reich, N. Patterson, and B. Berger (2013, May). Efficient moment-based  
1111 inference of admixture parameters and sources of gene flow. *Mol Biol Evol* 30(8), 1788–1802.
- 1112 Losos, J. B. (2011). Convergence, adaptation, and constraint. *Evolution* 65(7), 1827–1840.
- 1113 MacNair, M. R., S. E. Smith, and Q. J. Cumbes (1993, 11). Heritability and distribution of variation in  
1114 degree of copper tolerance in *mimulus guttatus* at copperopolis, california. *Heredity* 71(5), 445–455.
- 1115 Martin, A. and V. Orgogozo (2013). The loci of repeated evolution: a catalog of genetic hotspots of  
1116 phenotypic variation. *Evolution* 67(5), 1235–1250.
- 1117 Maynard Smith, J. (1971). What use is sex? *Journal of Theoretical Biology* 30(2), 319 – 335.
- 1118 Maynard Smith, J. and J. Haigh (1974, February). The hitch-hiking effect of a favourable gene. *Genet*  
1119 *Res* 23(1), 23–35.
- 1120 Nacci, D., L. Coiro, D. Champlin, S. Jayaraman, R. McKinney, T. R. Gleason, W. R. Munns Jr., J. L.  
1121 Specker, and K. R. Cooper (1999). Adaptations of wild populations of the estuarine fish *fundulus hetero-*  
1122 *clitus* to persistent environmental contaminants. *Marine Biology* 134(1), 9–17.

- 1123 Nacci, D. E., D. Champlin, and S. Jayaraman (2010). Adaptation of the estuarine fish *fundulus heteroclitus*  
1124 (atlantic killifish) to polychlorinated biphenyls (pcbs). *Estuaries and Coasts* 33(4), 853–864.
- 1125 Nicholson, G., A. V. Smith, F. Jónsson, Ó. Gústafsson, K. Stefánsson, and P. Donnelly (2002). Assessing  
1126 population differentiation and isolation from single-nucleotide polymorphism data. *Journal of the Royal*  
1127 *Statistical Society: Series B (Statistical Methodology)* 64(4), 695–715.
- 1128 Nielsen, R., S. Williamson, Y. Kim, M. Hubisz, A. Clark, and C. Bustamante (2005). Genomic scans for  
1129 selective sweeps using SNP data. *Genome Res.* 15, 1566–1575.
- 1130 Orr, H. A. (2005, January). The probability of parallel evolution. *Evolution* 59(1), 216–220.
- 1131 Pearce, R. J., H. Pota, M.-S. B. Evehe, E.-H. Bâ, G. Mombo-Ngoma, A. L. Malisa, R. Ord, W. Inojosa,  
1132 A. Matondo, D. A. Diallo, W. Mbacham, I. V. van den Broek, T. D. Swarthout, A. Getachew, S. Dejene,  
1133 M. P. Grobusch, F. Njie, S. Dunyo, M. Kweku, S. Owusu-Agyei, D. Chandramohan, M. Bonnet, J.-P.  
1134 Guthmann, S. Clarke, K. I. Barnes, E. Streat, S. T. Katokele, P. Uusiku, C. O. Agboghroma, O. Y.  
1135 Elegba, B. Cissé, I. E. A-Elbasit, H. A. Giha, S. P. Kachur, C. Lynch, J. B. Rwakimari, P. Chanda,  
1136 M. Hawela, B. Sharp, I. Naidoo, and C. Roper (2009, 04). Multiple origins and regional dispersal of  
1137 resistant *dhps* in African *Plasmodium falciparum* malaria. *PLoS Med* 6(4), e1000055.
- 1138 Pease, J. B., D. C. Haak, M. W. Hahn, and L. C. Moyle (2016). Phylogenomics reveals three sources of  
1139 adaptive variation during a rapid radiation. *PLoS Biol* 14(2), e1002379.
- 1140 Pennings, P. S. and J. Hermisson (2006, May). Soft sweeps ii—molecular population genetics of adaptation  
1141 from recurrent mutation or migration. *Mol Biol Evol* 23(5), 1076–1084.
- 1142 Przeworski, M., G. Coop, and J. D. Wall (2005). The signature of positive selection on standing genetic  
1143 variation. *Evolution* 59(11), 2312–2323.
- 1144 Racimo, F. (2016). Testing for ancient selection using cross-population allele frequency differentiation.  
1145 *Genetics* 202(2), 733–750.
- 1146 Racimo, F., S. Sankararaman, R. Nielsen, and E. Huerta-Sánchez (2015). Evidence for archaic adaptive  
1147 introgression in humans. *Nature Reviews Genetics* 16(6), 359–371.
- 1148 Reid, N. M., D. A. Proestou, B. W. Clark, W. C. Warren, J. K. Colbourne, J. R. Shaw, S. I. Karchner,  
1149 M. E. Hahn, D. Nacci, M. F. Oleksiak, D. L. Crawford, and A. Whitehead (2016). The genomic landscape  
1150 of rapid repeated evolutionary adaptation to toxic pollution in wild fish. *Science* 354(6317), 1305–1308.
- 1151 Roesti, M., S. Gavrillets, A. P. Hendry, W. Salzburger, and D. Berner (2014). The genomic signature of  
1152 parallel adaptation from shared genetic variation. *Molecular ecology* 23(16), 3944–3956.
- 1153 Rosenzweig, B. K., J. B. Pease, N. J. Besansky, and M. W. Hahn (2016). Powerful methods for detecting  
1154 introgressed regions from population genomic data. *Molecular Ecology* 25(11), 2387–2397.
- 1155 Samanta, S., Y.-J. Li, and B. S. Weir (2009). Drawing inferences about the coancestry coefficient. *Theoretical*  
1156 *Population Biology* 75(4), 312–9.
- 1157 Santiago, E. and A. Caballero (2005). Variation after a selective sweep in a subdivided population. *Genet-*  
1158 *ics* 169, 475–483.
- 1159 Slatkin, M. and T. Wiehe (1998). Genetic hitch-hiking in a subdivided population. *Genetical research* 71(02),  
1160 155–160.
- 1161 Song, Y., S. Endepols, N. Klemann, D. Richter, F.-R. Matuschka, C.-H. Shih, M. W. Nachman, and M. H.  
1162 Kohn (2011). Adaptive introgression of anticoagulant rodent poison resistance by hybridization between  
1163 old world mice. *Current Biology* 21(15), 1296–1301.
- 1164 Stern, D. L. (2013, 11). The genetic causes of convergent evolution. *Nat Rev Genet* 14(11), 751–764.

- 1165 Thompson, E. A. (2013). Identity by descent: Variation in meiosis, across genomes, and in populations.  
1166 *Genetics* 194(2), 301–326.
- 1167 Tishkoff, S. A., F. A. Reed, A. Ranciaro, B. F. Voight, C. C. Babbitt, J. S. Silverman, K. Powell, H. M.  
1168 Mortensen, J. B. Hirbo, M. Osman, M. Ibrahim, S. A. Omar, G. Lema, T. B. Nyambo, J. Ghorri, S. Bump-  
1169 stead, J. K. Pritchard, G. A. Wray, and P. Deloukas (2007, Jan). Convergent adaptation of human lactase  
1170 persistence in Africa and Europe. *Nat Genet* 39(1), 31–40.
- 1171 Turner, T., E. Bourne, E. V. Wettberg, T. Hu, and S. Nuzhdin (2010, January). Population resequencing  
1172 reveals local adaptation of *Arabidopsis lyrata* to serpentine soils. *Nat. Genet.* 42(3), 260–3.
- 1173 Varin, C., N. Reid, and D. Firth (2011). An overview of composite likelihood methods. *Statistica Sinica*,  
1174 5–42.
- 1175 Weir, B. S. and W. G. Hill (2002). Estimating F-statistics. *Annual Review of Genetics* 36, 721–50.
- 1176 Welch, J. J. and C. D. Jiggins (2014). Standing and flowing: the complex origins of adaptive variation.  
1177 *Molecular Ecology* 23(16), 3935–3937.
- 1178 Wiuf, C. (2006). Consistency of estimators of population scaled parameters using composite likelihood.  
1179 *Journal of mathematical biology* 53(5), 821–841.
- 1180 Wood, T. E., J. M. Burke, and L. H. Rieseberg (2005, 02). Parallel genotypic adaptation: when evolution  
1181 repeats itself. *Genetica* 123(1-2), 157–170.
- 1182 Wright, K. M., U. Hellsten, C. Xu, A. L. Jeong, A. Sreedasyam, J. A. Chapman, J. Schmutz, G. Coop, D. S.  
1183 Rokhsar, and J. H. Willis (2015). Adaptation to heavy-metal contaminated environments proceeds via  
1184 selection on pre-existing genetic variation. *bioRxiv*.
- 1185 Wright, S. (1943). Isolation by distance. *Genetics* 28(2), 114.
- 1186 Wright, S. (1951, March). The genetical structure of populations. *Annals of Eugenics* 15(4), 323–354.

1187 **S1 Supplemental tables and figures**



(a) MCLE of **selection coefficients** as function of true location of selected site. Each location of selected site has 100 simulations under **independent mutation model** (10 chromosomes per population,  $N_e = 100,000$ ,  $s = 0.05$ ). Crossbars indicate first and third quartiles with second quartiles (medians) as the horizontal line. The true values of the parameters are marked with dashed, black lines.

(b) MCLE of **selection coefficients** versus MCLE of **location of selected site**. True location of selected site is marked by color. Each location of selected site has 100 simulations under **independent mutation model** (10 chromosomes per population,  $N_e = 100,000$ ,  $s = 0.05$ )

Figure S1: MCLE of **parameters for independent mutation simulations allowing selected site to vary**.

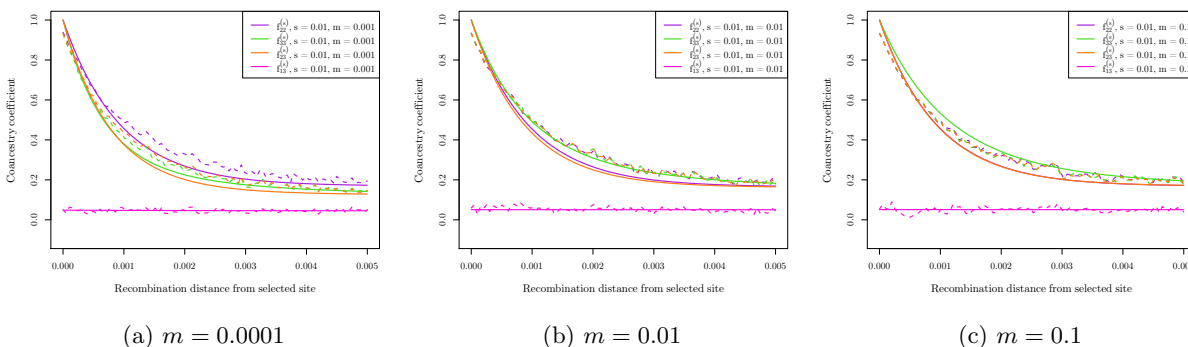
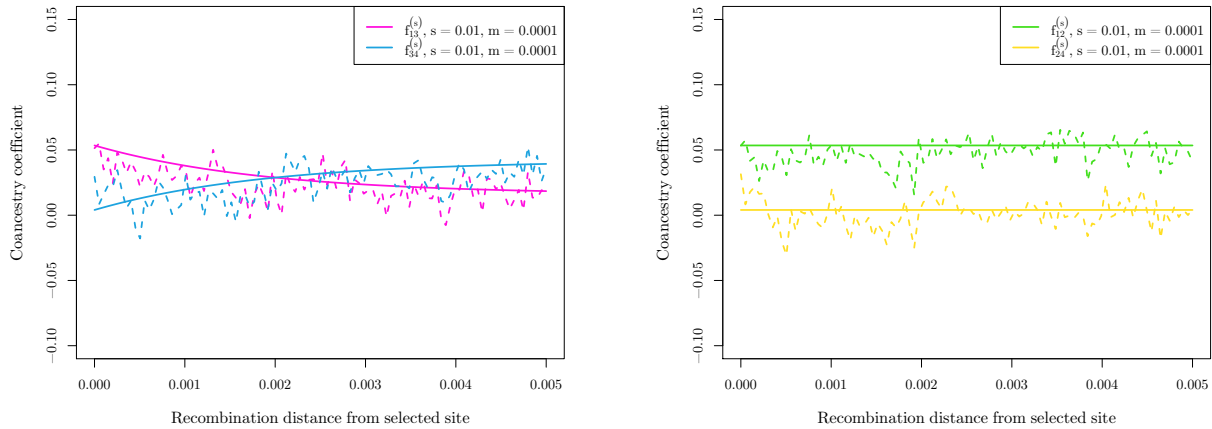


Figure S2: Average coancestry coefficient values for migration simulations with various  $m$ , across 100 runs of simulations for each of 100 bins of distance away from the selected site, showing the migration rate parameter does not have a large effect on both expectations (solid lines) and simulation results (dashed lines). For all simulations,  $s = 0.01$ ,  $N_e = 10,000$ , and the source of the beneficial allele is population 2.

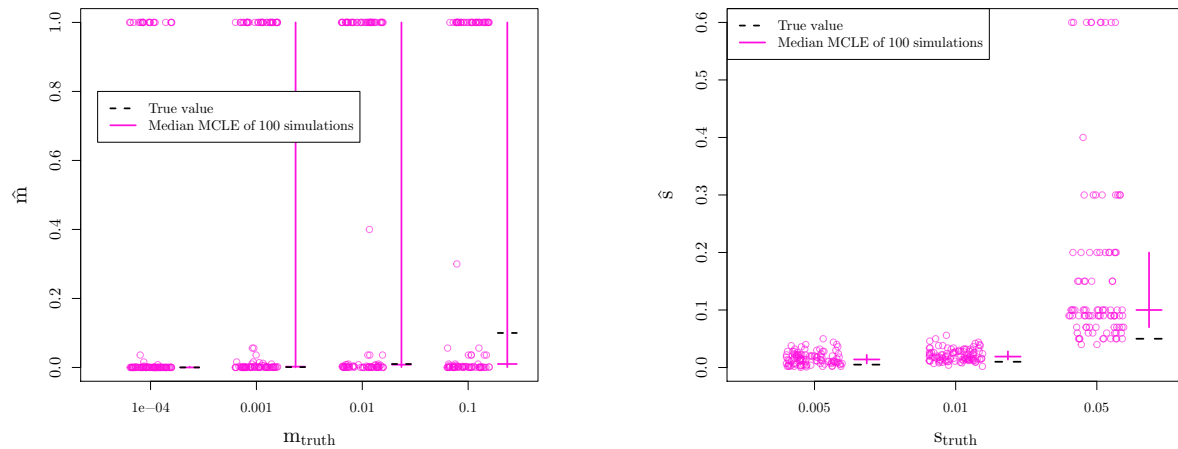




(a) Average coancestry coefficient values for migration simulations across 100 runs of simulations for each of 100 bins of distance away from the selected site, between recipient population (3) and non-selected populations (1 and 4).

(b) Average coancestry coefficient values for migration simulations across 100 runs of simulations for each of 100 bins of distance away from the selected site, between source population (2) and non-selected populations (1 and 4).

Figure S3: Average coancestry coefficient values for migration simulations across 100 runs of simulations for each of 100 bins of distance away from the selected site, between source and recipient populations and non-selected populations ( $s = 0.01$ ,  $m = 0.001$ ,  $N_e = 10,000$ ).



(a) MCLE of **migration rates** for 100 simulations under **migration model** (10 chromosomes per population,  $N_e = 10,000$ ,  $s = 0.01$ )

(b) MCLE of **selection coefficients** for 100 simulations under **migration model** (10 chromosomes per population,  $N_e = 10,000$ ,  $m = 0.001$ )

Figure S4: MCLE of **parameters** for **migration model** simulations. We vary the true value of the parameter used for simulations along the x-axis and show the MCLE for each of 100 simulations (points). Crossbars indicate first and third quartiles with second quartiles (medians) as the horizontal line. The true values of the parameters are marked with dashed, black lines.

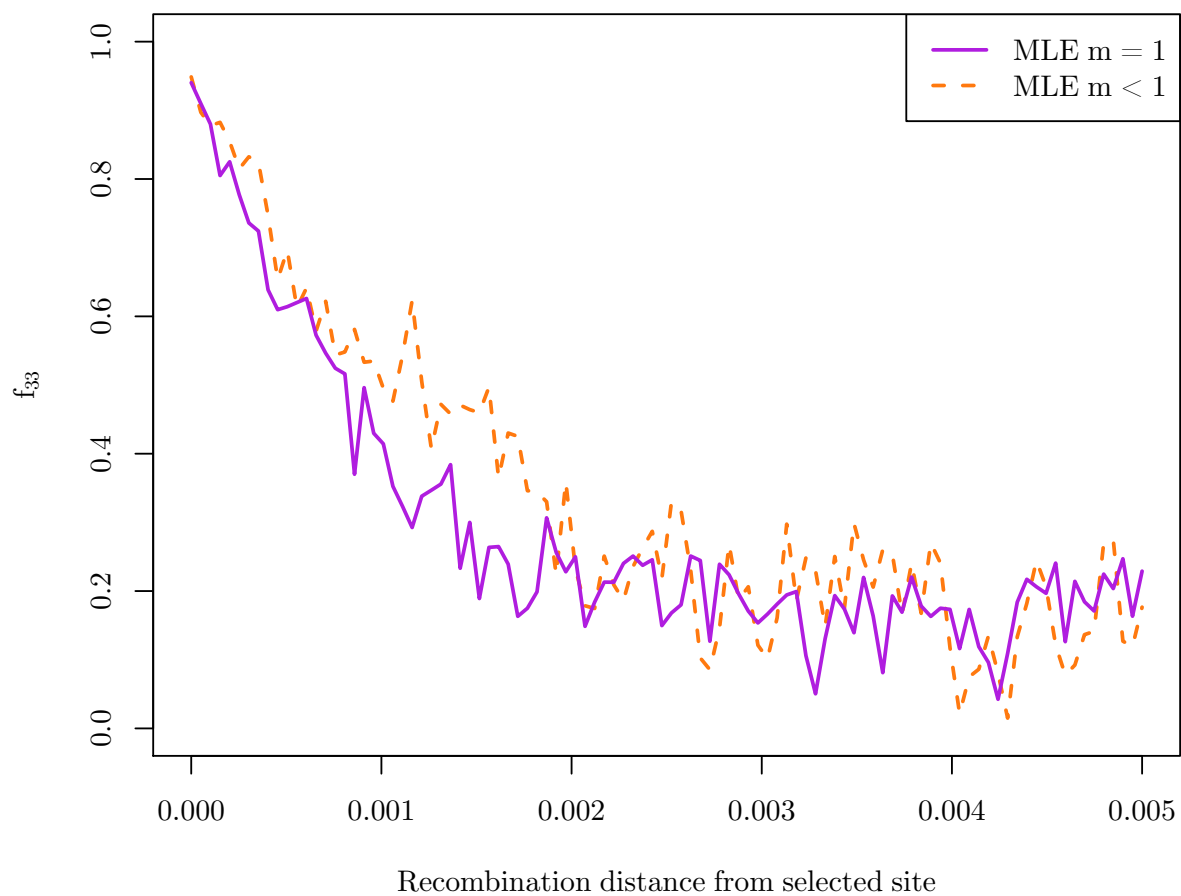


Figure S5: Coancestry coefficient for the recipient population as a function of recombination distance from the selected site, partitioned into simulations with MLE for  $m = 1$  and  $m < 1$  ( $s = 0.01$ ,  $m = 0.001$ ,  $N_e = 10,000$ ).

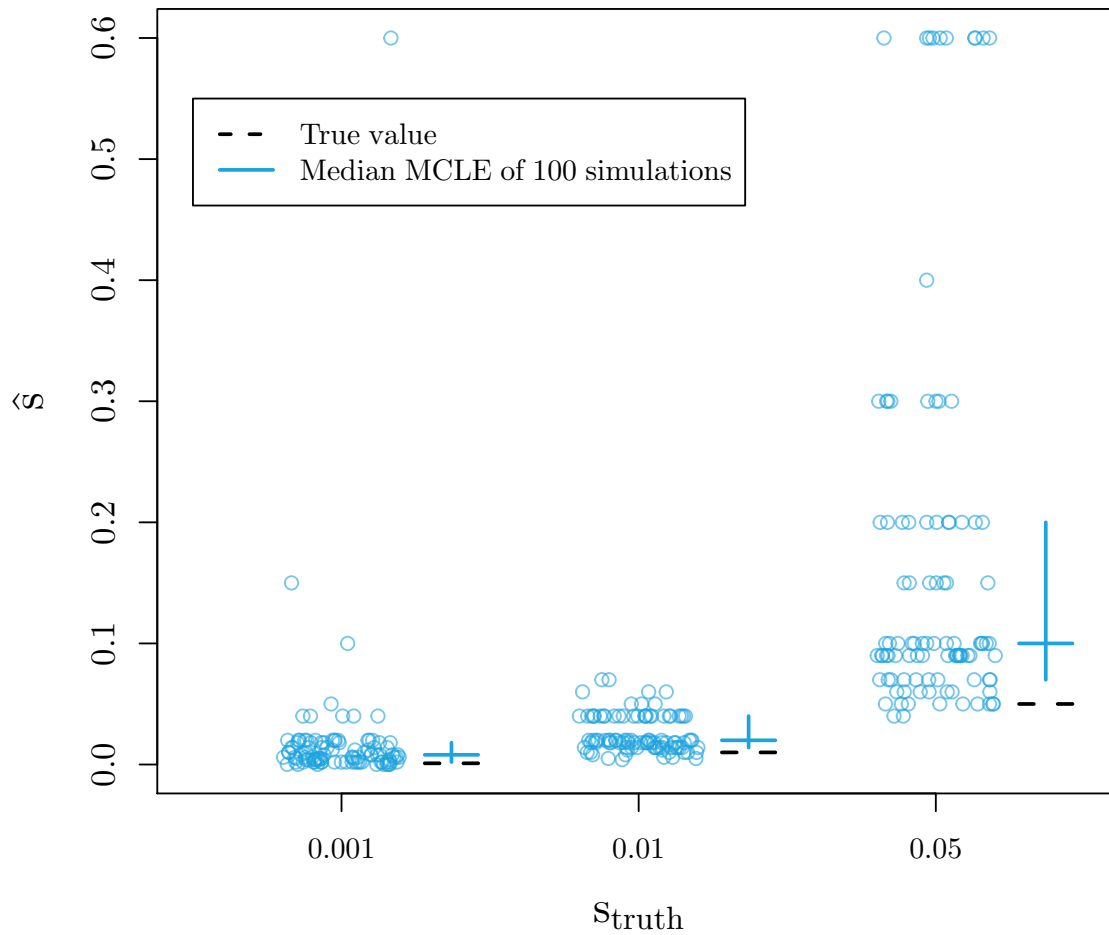
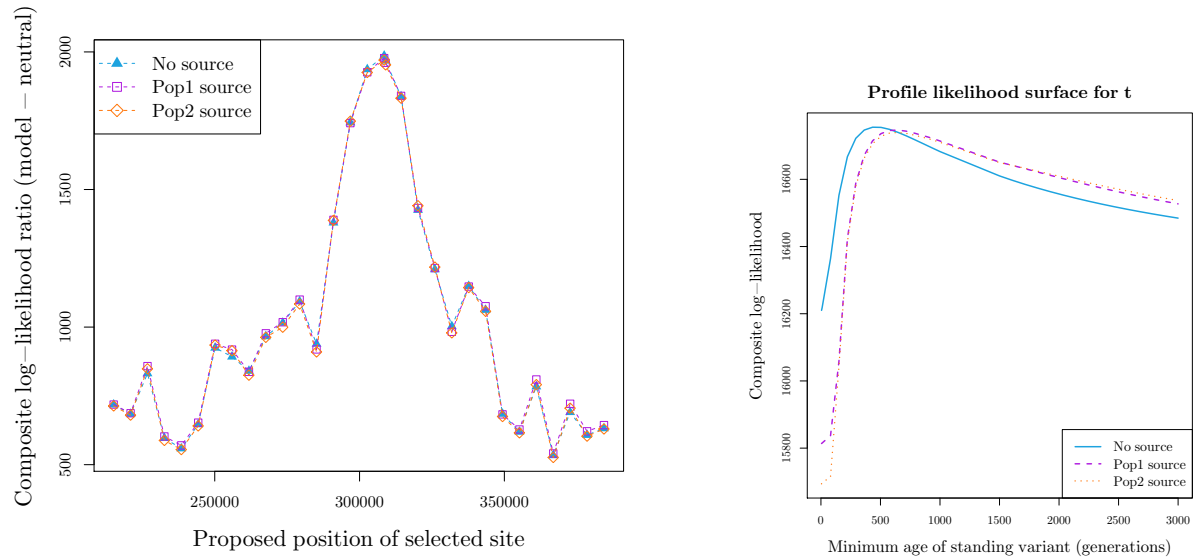


Figure S6: MCLE of **selection coefficients** for 100 simulations under **standing variant model** (10 chromosomes per population,  $N_e = 10,000$ ,  $t = 500$ ,  $g = 0.001$ ). We vary the true value of the parameter used for simulations along the x-axis and show the MCLE for each of 100 simulations (points). Crossbars indicate first and third quartiles with second quartiles (medians) as the horizontal line. The true values of the parameters are marked with dashed, black lines.



(a) Composite log-likelihood for standing variation model with no source specified and both selected populations as potential sources, as a function of the proposed selected site.

(b) Profile composite log-likelihood of the minimum age of the standing variant for standing variant model with no source specified and both selected populations as potential sources.

Figure S7: Inference results for standing variant model applied to *Mimulus* data using both original standing variant model and more complex model where a source population is specified. In this case, the composite log-likelihoods do not change, but the parameter estimates do. We obtain higher MLE for  $t$  when a source is specified (646 generations) compared to the original no source model (434 generations). This fits our expectation as  $t$  has slightly different interpretations under the two models.

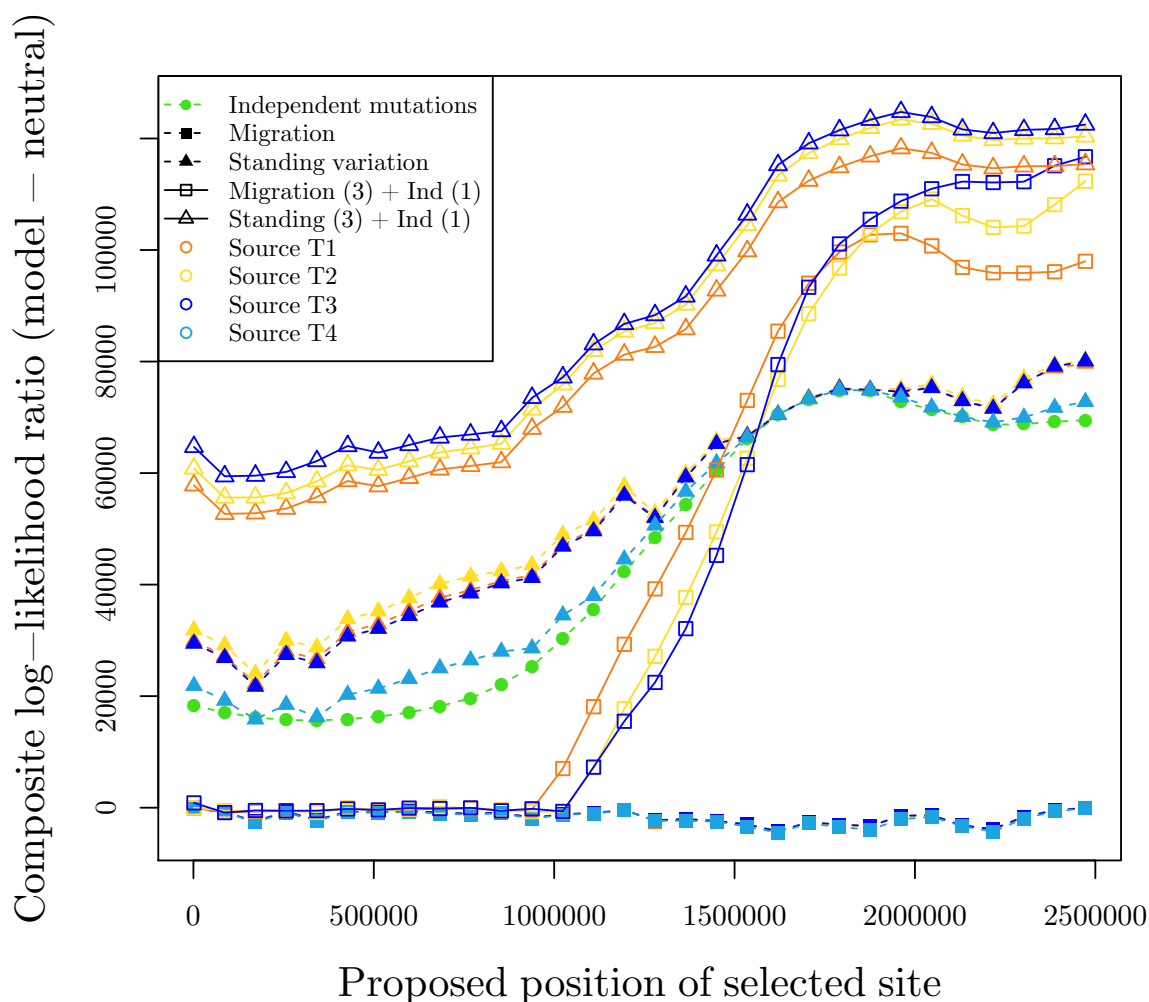


Figure S8: Composite log-likelihood for *Fundulus heteroclitus* pollutant tolerance adaptation on Scaffold9893, showing all possible sources for models with migration and standing variant model, as a function of the proposed selected site.

Table S1: Parameter spaces for composite likelihood calculations for simulated datasets

Position of selected site	0
$s$	$10^{-4}$ , $5 \times 10^{-4}$ , $10^{-3}$ , $2 \times 10^{-3}$ , $4 \times 10^{-3}$ , $5 \times 10^{-3}$ , $6 \times 10^{-3}$ , $8 \times 10^{-3}$ , 0.01, 0.012, 0.014, 0.018, 0.02, 0.03, 0.04, 0.05, 0.06, 0.07, 0.09, 0.1, 0.11, 0.12, 0.14, 0.15, 0.2, 0.25, 0.3, 0.35, 0.4, 0.5, 0.6
$t$	0, 5, 15, 25, 40, 50, 60, 75, 100, 150, 200, 250, 300, 350, 400, 450, 500, 550, 600, 650, 700, 750, 800, 900, 1000, 1200, 1500, 1800, 2000, 2500, 3000, 3500, 4000, 4500, 5000, 5500, 6000, 6500, 7000, 7500, 8000, 9000, $10^4$ , $1.5 \times 10^5$ , $2 \times 10^5$ , $3 \times 10^5$ , $5 \times 10^5$ , $7 \times 10^5$ , $9 \times 10^5$ , $10^6$
$g$	$10^{-3}$
$m$	$10^{-5}$ , $10^{-4}$ , $5 \times 10^{-4}$ , $10^{-3}$ , $5 \times 10^{-3}$ , 0.01, 0.2, 0.5, 0.9, 1
Migration source population	2

Table S2: Parameter spaces for composite likelihood calculations for independent sweep model simulations

Position of selected site	0
<i>s</i>	$10^{-4}$ , $2 \times 10^{-4}$ , $3 \times 10^{-4}$ , $4 \times 10^{-4}$ , $5 \times 10^{-4}$ , $6 \times 10^{-4}$ , $7 \times 10^{-4}$ , $8 \times 10^{-4}$ , $9 \times 10^{-4}$ , 0.001, 0.0015, 0.002, 0.0025, 0.003, 0.0035, 0.004, 0.0045, 0.005, 0.0055, 0.006, 0.0065, 0.007, 0.0075, 0.008, 0.0085, 0.009, 0.0095, 0.01, 0.0105, 0.011, 0.0115, 0.012, 0.0125, 0.013, 0.0135, 0.014, 0.0145, 0.015, 0.0155, 0.016, 0.0165, 0.017, 0.0175, 0.018, 0.0185, 0.019, 0.0195, 0.02, 0.0205, 0.021, 0.0215, 0.022, 0.0225, 0.023, 0.0235, 0.024, 0.0245, 0.025, 0.0255, 0.026, 0.0265, 0.027, 0.0275, 0.028, 0.0285, 0.029, 0.0295, 0.03, 0.0305, 0.031, 0.0315, 0.032, 0.0325, 0.033, 0.0335, 0.034, 0.0345, 0.035, 0.0355, 0.036, 0.0365, 0.037, 0.0375, 0.038, 0.0385, 0.039, 0.0395, 0.04, 0.0405, 0.041, 0.0415, 0.042, 0.0425, 0.043, 0.0435, 0.044, 0.0445, 0.045, 0.0455, 0.046, 0.0465, 0.047, 0.0475, 0.048, 0.0485, 0.049, 0.0495, 0.05, 0.0505, 0.051, 0.0515, 0.052, 0.0525, 0.053, 0.0535, 0.054, 0.0545, 0.055, 0.0555, 0.056, 0.0565, 0.057, 0.0575, 0.058, 0.0585, 0.059, 0.0595, 0.06, 0.0605, 0.061, 0.0615, 0.062, 0.0625, 0.063, 0.0635, 0.064, 0.0645, 0.065, 0.0655, 0.066, 0.0665, 0.067, 0.0675, 0.068, 0.0685, 0.069, 0.0695, 0.07, 0.0705, 0.071, 0.0715, 0.072, 0.0725, 0.073, 0.0735, 0.074, 0.0745, 0.075, 0.0755, 0.076, 0.0765, 0.077, 0.0775, 0.078, 0.0785, 0.079, 0.0795, 0.08, 0.0805, 0.081, 0.0815, 0.082, 0.0825, 0.083, 0.0835, 0.084, 0.0845, 0.085, 0.0855, 0.086, 0.0865, 0.087, 0.0875, 0.088, 0.0885, 0.089, 0.0895, 0.09, 0.0905, 0.091, 0.0915, 0.092, 0.0925, 0.093, 0.0935, 0.094, 0.0945, 0.095, 0.0955, 0.096, 0.0965, 0.097, 0.0975, 0.098, 0.0985, 0.099, 0.0995, 0.1, 0.1005, 0.101, 0.1015, 0.102, 0.1025, 0.103, 0.1035, 0.104, 0.1045, 0.105, 0.1055, 0.106, 0.1065, 0.107, 0.1075, 0.108, 0.1085, 0.109, 0.1095, 0.11, 0.1105, 0.111, 0.1115, 0.112, 0.1125, 0.113, 0.1135, 0.114, 0.1145, 0.115, 0.1155, 0.116, 0.1165, 0.117, 0.1175, 0.118, 0.1185, 0.119, 0.1195, 0.12, 0.1205, 0.121, 0.1215, 0.122, 0.1225, 0.123, 0.1235, 0.124, 0.1245, 0.125, 0.1255, 0.126, 0.1265, 0.127, 0.1275, 0.128, 0.1285, 0.129, 0.1295, 0.13, 0.1305, 0.131, 0.1315, 0.132, 0.1325, 0.133, 0.1335, 0.134, 0.1345, 0.135, 0.1355, 0.136, 0.1365, 0.137, 0.1375, 0.138, 0.1385, 0.139, 0.1395, 0.14, 0.1405, 0.141, 0.1415, 0.142, 0.1425, 0.143, 0.1435, 0.144, 0.1445, 0.145, 0.1455, 0.146, 0.1465, 0.147, 0.1475, 0.148, 0.1485, 0.149, 0.1495, 0.15, 0.16, 0.17, 0.18, 0.19, 0.2, 0.21, 0.22, 0.23, 0.24, 0.25, 0.26, 0.27, 0.28, 0.29, 0.3, 0.31, 0.32, 0.33, 0.34, 0.35, 0.36, 0.37, 0.38, 0.39, 0.4, 0.41, 0.42, 0.43, 0.44, 0.45, 0.46, 0.47, 0.48, 0.49, 0.5, 0.51, 0.52, 0.53, 0.54, 0.55, 0.56, 0.57, 0.58, 0.59, 0.6

Table S3: Parameter spaces for composite likelihood calculations for independent sweep model simulations when position of selected site varies

Position of selected site	0, 0.01, 0.02, 0.04, 0.06, 0.08, 0.1, 0.12, 0.14, 0.16, 0.18, 0.2, 0.22, 0.24, 0.26, 0.28, 0.3, 0.32, 0.34, 0.36, 0.38, 0.4, 0.42, 0.44, 0.46, 0.48, 0.5, 0.52, 0.54, 0.56, 0.58, 0.6, 0.62, 0.64, 0.66, 0.68, 0.7, 0.72, 0.74, 0.76, 0.78, 0.8, 0.82, 0.84, 0.86, 0.88, 0.9, 0.92, 0.94, 0.96, 0.98, 1
<i>s</i>	$10^{-4}$ , $5 \times 10^{-4}$ , 0.001, 0.002, 0.004, 0.005, 0.006, 0.008, 0.01, 0.012, 0.014, 0.018, 0.02, 0.03, 0.04, 0.05, 0.06, 0.07, 0.09, 0.1, 0.11, 0.12, 0.14, 0.15, 0.2, 0.25, 0.3, 0.35, 0.4, 0.5, 0.6

Table S4: Parameter spaces for composite likelihood calculations for migration model simulations

Position of selected site	0
$s$	$10^{-4}$ , 0.001, 0.002, 0.003, 0.004, 0.005, 0.006, 0.007, 0.008, 0.009, 0.01, 0.011, 0.012, 0.013, 0.014, 0.015, 0.016, 0.018, 0.02, 0.022, 0.024, 0.026, 0.028, 0.03, 0.032, 0.034, 0.036, 0.038, 0.04, 0.042, 0.044, 0.046, 0.048, 0.05, 0.052, 0.054, 0.056, 0.058, 0.06, 0.062, 0.064, 0.066, 0.068, 0.07, 0.08, 0.09, 0.1, 0.11, 0.12, 0.13, 0.14, 0.15, 0.2, 0.3, 0.4, 0.5, 0.6
$m$	$1^{-5}$ , $8 \times 10^{-5}$ , $0^{-4}$ , $1.2 \times 10^{-4}$ , $1.4 \times 10^{-4}$ , $1.6 \times 10^{-4}$ , $1.8 \times 10^{-4}$ , $2 \times 10^{-4}$ , $2.2 \times 10^{-4}$ , $2.4 \times 10^{-4}$ , $2.6 \times 10^{-4}$ , $2.8 \times 10^{-4}$ , $3 \times 10^{-4}$ , $3.2 \times 10^{-4}$ , $3.4 \times 10^{-4}$ , $3.6 \times 10^{-4}$ , $3.8 \times 10^{-4}$ , $4 \times 10^{-4}$ , $8 \times 10^{-4}$ , 0.001, 0.0012, 0.0014, 0.0016, 0.0018, 0.002, 0.0022, 0.0024, 0.0026, 0.0028, 0.003, 0.0032, 0.0034, 0.0036, 0.0038, 0.004, 0.006, 0.008, 0.01, 0.012, 0.014, 0.016, 0.036, 0.056, 0.076, 0.096, 0.116, 0.136, 0.156, 0.176, 0.196, 0.3, 0.4, 0.5, 0.6, 0.7, 0.8, 0.9, 1
Migration source population	2

Table S5: Parameter spaces for composite likelihood calculations for standing variation model simulations

Position of selected site	0
$s$	$10^{-4}$ , 0.0020, 0.0040, 0.0050, 0.0060, 0.0080, 0.0100, 0.0120, 0.0140, 0.0180, 0.0200, 0.0400, 0.0500, 0.0600, 0.0700, 0.0900, 0.1000, 0.1500, 0.2000, 0.3000, 0.4000 0.5000 0.6000
$t$	5, 5, 25, 40, 50, 60, 75, 100, 150, 200, 250, 300, 350, 400, 450, 500, 550, 600, 650, 700, 750, 800, 900, 1000, 1500, 2000, 2500, 3000, 3500, 4000, 4500, 5000, 5500, 6000, 6500, 7000, 7500, 8000, 9000, 10000, 15000, 20000, 30000, 50000, 70000, 9000, $10^5$
$g$	$10^{-6}$ , $10^{-5}$ , $10^{-4}$ , $10^{-3}$ , $10^{-2}$

Table S6: Neutral  $\mathbf{F}$  matrix from 12 scaffolds with no strong signatures of selection in *Mimulus guttatus* populations (Scaffold7 and regions adjacent to scaffolds 1, 4, 8, 47, 80, 84, 106, 115, 129, 148, 198). Populations 1 and 3 are copper tolerant.

	Pop1	Pop2	Pop3	Pop4
Pop1	0.1571	0.0266	0.0153	0.0356
Pop2	0.0266	0.1008	0.0000	0.0204
Pop3	0.0153	0.0000	0.1807	0.0179
Pop4	0.0356	0.0204	0.0179	0.1232

Table S7: Parameter spaces for composite likelihood calculations for *Mimulus*

Position of selected site	215100, 220938, 226775, 232613, 238451, 244289, 250126, 255964, 261802, 267640, 273477, 279315, 285153, 290990, 296828, 302666, 308504, 309000, 314341, 320179, 326017, 331854, 337692, 343530, 349368, 355205, 361043
$s$	0.001, 0.002, 0.003, 0.004, 0.005, 0.006, 0.007, 0.008, 0.009, 0.01, 0.011, 0.014, 0.016, 0.019, 0.021, 0.024, 0.026, 0.029, 0.032, 0.034, 0.037, 0.039, 0.042, 0.045, 0.047, 0.05, 0.052, 0.055, 0.057, 0.06, 0.08, 0.1, 0.15, 0.2, 0.25, 0.3, 0.35, 0.4, 0.45, 0.5, 0.55, 0.6
$t$	5, 10, 81, 151, 222, 293, 364, 434, 505, 576, 646, 717, 788, 859, 929, 1000, 1500, 1607, 1714, 1821, 1929, 2036, 2143, 2250, 2357, 2464, 2571, 2679, 2786, 2893, 3000
$g$	$10^{-10}$ , $10^{-9}$ , $10^{-8}$ , $10^{-7}$ , $10^{-6}$ , $10^{-5}$ , $10^{-4}$ , $10^{-3}$ , $10^{-2}$
$m$	$10^{-5}$ , $10^{-4}$ , $5^{-4}$ , 0.001, 0.005, 0.01, 0.1, 0.2, 0.3, 0.4, 0.5, 0.6, 0.7, 0.8, 0.9, 1
Migration source population	1, 3

Table S8: Neutral  $\mathbf{F}$  matrix from four scaffolds with no strong signatures of selection in *Fundulus heteroclitus* populations (Scaffold0, Scaffold1, Scaffold2, Scaffold3)

	S1	T1	S2	T2	S3	T4	S5	T5
S1	0.339	0.292	0.315	0.332	0.179	0.229	0.022	0.003
T1	0.292	0.372	0.304	0.329	0.171	0.218	0.020	0.000
S2	0.315	0.304	0.381	0.384	0.213	0.263	0.053	0.034
T2	0.332	0.329	0.384	0.451	0.220	0.276	0.055	0.035
S3	0.179	0.171	0.213	0.220	0.198	0.192	0.058	0.044
T3	0.229	0.218	0.263	0.276	0.192	0.272	0.053	0.037
S4	0.022	0.020	0.053	0.055	0.058	0.053	0.142	0.093
T4	0.003	0.000	0.034	0.035	0.044	0.037	0.093	0.142

Table S9: Parameter spaces for composite likelihood calculations for *Fundulus*

Position of selected site	1452, 86658, 171865, 257071, 342277, 427484, 512690, 597896, 683103, 768309, 853515, 938722, 1023928, 1109134, 1194341, 1279547, 1364754, 1449960, 1535166, 1620373, 1705579, 1790785, 1875992, 1961198, 2046404, 2131611, 2216817, 2302023, 2387230, 2472436
$s$	0.001, 0.005, 0.01, 0.02, 0.03, 0.04, 0.05, 0.06, 0.08, 0.1, 0.12, 0.14, 0.16, 0.18, 0.2, 0.3, 0.4, 0.5, 0.6
$t$	0, 5, 50, 100, 500, 1000, 5000, $10^7$
$g$	$10^{-10}$ , $10^{-9}$ , $10^{-8}$ , $10^{-7}$ , $10^{-6}$ , $10^{-5}$ , $10^{-4}$ , $10^{-3}$ , $10^{-2}$
$m$	$10^{-5}$ , $10^{-4}$ , $5^{-4}$ , 0.001, 0.005, 0.01, 0.1, 0.3, 0.5, 0.9, 1
Source population	T1, T2, T3, T4